Chapter 16
Radar Time Series for Land Cover and Forest Mapping

Christiane Schmullius, Christian Thiel, Carsten Pathe, and Maurizio Santoro

Abstract Radar time series are powerful means to improve retrieval algorithms about land surface characteristics in the following ways: (i) as information for identification of land surface conditions, (ii) as source of multivariate statistics for mapping methodologies, (iii) to select the right scene(s) for dedicated retrieval procedures, or (iv) to train model parameters in physical retrievals. Albeit radar data from air- and spaceborne platforms have been investigated since 40 years, operational applications are limited – partly due to the non-intuitive handling of complex microwave backscatter signals, and partly due to restricted geometric and temporal resolutions or frequency and polarization constraints. This chapter gives an overview of 20 years of pilot projects performed by the authors and their collaborators with the goal of large-area radar data exploration. All studies lead to innovative pre-operational applications, several with promising discoveries that can now be realized with a new and expanding fleet of radar satellites. Four case studies for land cover, forest mapping, forest cover change and savannah monitoring conclude this chapter.

16.1 Introduction

Radar remote sensing applications for land surfaces have been investigated extensively since the 1980s, when NASA deployed their airborne system AIRSAR over various test sites to prepare and accompany a series of spaceborne Shuttle Imaging Radar (SIR) experiments (1981: SIR-A, 1984: SIR-B, April and October 1994: SIR-C/X-SAR) jointly with the German Aerospace Centre (DLR) and the Italian

C. Schmullius (✉) • C. Thiel • C. Pathe
Department for Earth Observation, Institute of Geography, Faculty for Chemistry and Geosciences, Friedrich-Schiller University, Jena, Germany
e-mail: c.schmullius@uni-jena.de

M. Santoro
GAMMA Remote Sensing Research and Consulting AG, Gümligen, Switzerland

C. Kuenzer et al. (eds.), *Remote Sensing Time Series*, Remote Sensing and Digital Image Processing, DOI 10.1007/978-3-319-15967-6_16

Space Agency (ASI). These Multi-sensor Airborne Campaigns (MACs) and SIR-missions represent the first proof-of-concept of retrievals which have been developed with ground scatterometer systems in the decades before. A summary by Ulaby et al. 1986 of these in situ backscatter time series under various environmental conditions with explanations of the underlying physics still serves as a major reference for applications with spaceborne data. This transferability of concepts is based on the unique radar calibration procedure which allows comparisons over time and between sensors as long as the same wavelength and polarisation is being used. The fundamental relation between the characteristics of the radar system, the transmitted signal, the target, and the received signal is called the radar equation. Since radar systems actively emit microwave radiation, the illuminating geometry and technical characteristics are known and can thus be accounted for in the retrieval algorithm for a specific surface phenomenon (such as phenological state, biomass, or soil moisture).

Albeit the information content in radar images corresponds to well-defined surface parameters (i.e. volumetric moisture, surface roughness and structure of the scattering medium), this remote sensing technique has only a limited user community due to the complexity of the necessary pre-processing steps. These procedures originate from the principle of using backscattered intensities of actively emitted microwave pulses, thus causing speckle, corner reflections or geometric obstacles such as layover, foreshortening and rectangular pixels – these are all non-intuitive phenomena for the optically trained remote sensing expert. Hence, radar image understanding needs specific training, especially for non-engineers. This gap has for example been tackled in the Radar remote sensing education initiative (SAR-EDU) of the German Space Administration (DLR Raumfahrtmanagement) which provides educational material to interested university teachers, federal agency employees and PhD students through a dedicated DLR web-portal since December 2014: https://saredu.dlr.de. The reader is referred to this portal for background material, since an introduction to radar theory would go beyond the scope of this section.

The following paragraphs contain an overview of three concepts of how to use radar time series as tools for land cover and forestry applications: (1) information about what + where + state of land surface characteristics, (2) source of multivariate statistics as mapping characteristics, (3) choosing the right scene for the product retrieval. Four examples of operational applications for land cover, forest cover and -change and savannah monitoring are given in the third section.

16.2 Radar Time Series as a Tool for Land Monitoring

Land surface properties unfold their characteristics in radar data sets – as for optical images – when exploiting temporal information. Time series are of special importance for radar applications because of the limited spectral space (usually only one wavelength and two polarisations) and because of the radar-specific suitability for

multi-temporal exploitation due to the sensor's high radiometric accuracies. Additionally, due to the capability of radar signals to penetrate the atmosphere even in the presence of clouds and rain, radar time series allow to focus on the changing surface constituents over months, years, and even decades as will be demonstrated.

16.2.1 Time Series for Information Retrieval About Land Cover State

Operational land cover mapping with spaceborne radar data became possible with the launch of the European satellite ERS-1 in 1991. For the first time, SAR images became available globally and repeatedly. A first summary publication by the European Space Agency (ESA) (Wooding et al. 1995) showed the remarkable behaviour of C-band VV-polarized time series for crop mapping (Fig. 16.1). Backscatter and attenuation features, already described in Ulaby et al. 1986 (ibid. Fig. 17.19.32, p. 1566), were now observable for large areas and thus their spatial manifestation was proven.

Global C-Band time series were successfully continued through the launches of ESA's follow-up satellites ERS-2 (European Remote Sensing) in 1995 and ASAR (Advanced Synthetic Aperture Radar) on ENVISAT (Environmental Satellite) in 2002. Providing over a decade of C-band data allowed the development of automated routines for land cover mapping. The German ENVILAND-1 and -2 projects, supported by DLR's Space Administration from 2004 to 2012, investigated the potential of radar-optical fusion techniques. The goal was the development of an automated retrieval of land cover and biophysical characteristics through exploitation of both sensor types. The proposed classification procedure consisted of three main stages. The first processing step comprises the segmentation of the optical Earth observation (EO) data. Next, potential training sites are being selected automatically by applying a decision tree with flexible, scene-specific thresholds that are calculated based on expert knowledge and histogram analyses. Finally, as the third step, training samples are being used as input to a supervised classification. The overall accuracy of the final land cover map increased by 6 % when C-band texture and backscatter information was included during classification. The results are illustrated in Fig. 16.2. A significant improvement was achieved for the classes Urban and Grassland as well as for Forest. The absolute number of crop classes could be increased (Riedel et al. 2008).

Radar time series not only support identification of phenological states and improve classification accuracies; they can also be used innovatively in cloud removal. Eckardt et al. (2013) reconstructed cloud-contaminated pixels in Landsat images using the Synthetic Aperture Radar (SAR) data. Cloud contamination was simulated with masks of varying size to systematically investigate the developed technique. The authors used three radar images during 1 month of the growing season to establish a small temporal signature. Each image, though, originated from

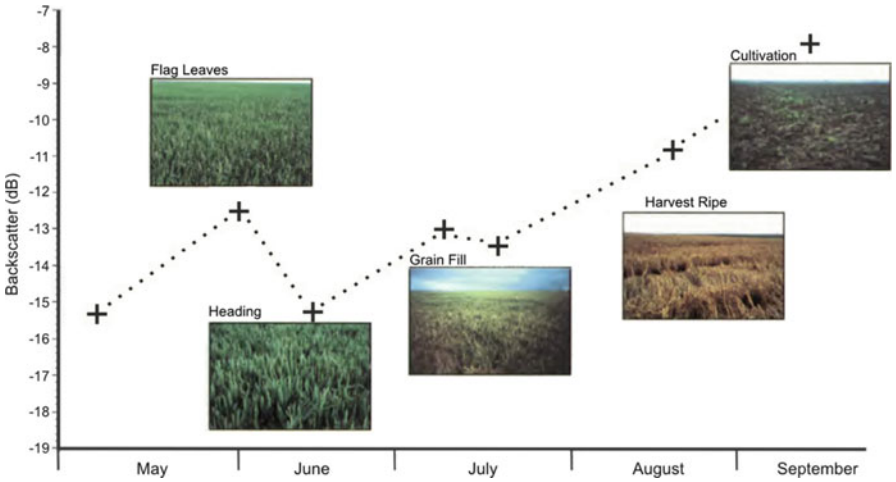

Fig. 16.1 Multi-temporal signature of ERS-1 C-band backscatter signals (Wooding et al. 1995, modified): the decrease between end of May and mid-June is characteristic for the increasing attenuation of VV-polarized radar pulses during the lengthening of cereal stalks or, similarly, grass canopies. With ripening and yellowing, attenuation is minimized and backscatter increases again. This process is especially observable at C-band because of the correspondence in size between the wavelength and geometry of the scattering objects

a different radar satellite (ERS-2, TerraSAR-X and ALOS-1 (Advanced Land Observing Satellite)). They developed a Closest Feature Vector (CFV) based on the assumption of a physical relation between reflectances in the VIS/NIR (Visible/near-infrared) part of the electromagnetic spectrum, the temporal microwave backscatter signature, and the respective plant conditions at the acquisition dates. SAR data thus guided the selection of the needed reflectances as an integral part of the processing procedure to fill cloudy image gaps. Figure 16.3 illustrates the information content of radar false-colour composites compared to a Landsat VIS-band colour composite.

16.2.2 Time Series as Source for Statistical Land Surface Indicators

Comparable to coarse resolution optical image acquisitions (e.g. Medium Resolution Imaging Spectrometer (MERIS), Satellite Pour l'Observation de la Terre-Vegetation (SPOT-VGT), National Oceanic and Atmospheric Administration (NOAA) Advanced Very High Resolution Radiometer (AVHRR)), new ScanSAR modes became available having a reduced geometric resolution but an improved temporal repetition rate. The first ScanSAR-mode from a satellite was provided from the Canadian RADARSAT-1 launched in 1995, followed by the ENVISAT ASAR system in 2002. These new types of data sets enabled continental, wall-to-

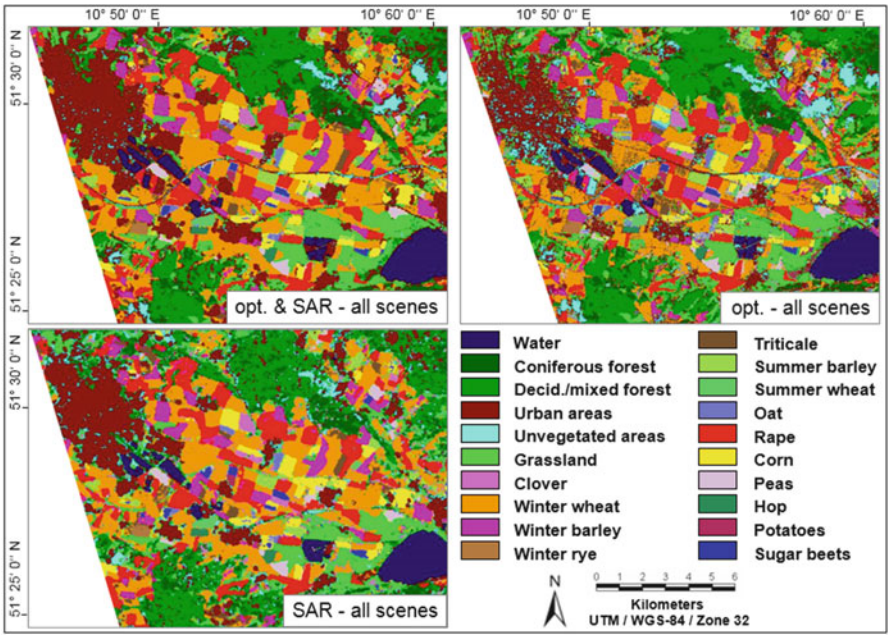

Fig. 16.2 Land cover maps from multi-temporal Landsat, ASAR and ERS-2 scenes from 2005, test site Nordhausen/Thuringia, Germany. The achieved overall accuracies are: optical & SAR: 83,7 %; optical only: 77,9 %; SAR only: 80,2 % (© Uni Jena, 2007). Only two Landsat scenes from 21. April and 10. July were available due to typical cloudy weather conditions during the growing season, but nine SAR images could be used

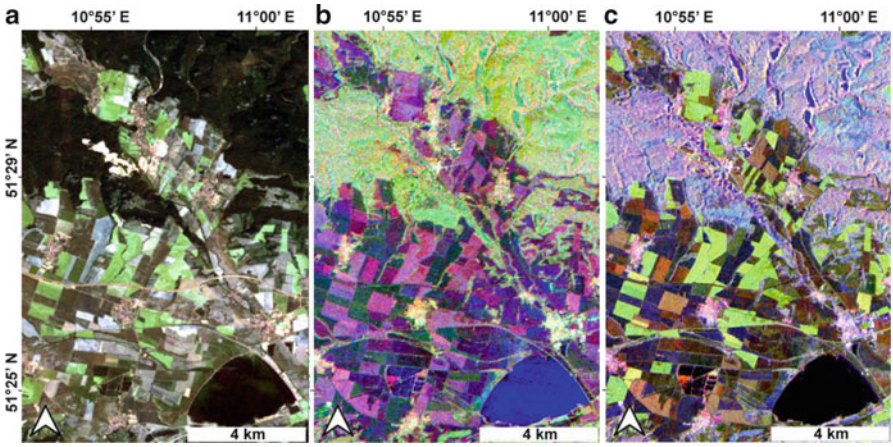

Fig 16.3 Comparison of colour composites to illustrate the image information content: (**a**) Landsat TM5 B3|B2|B1; (**b**) X-HH|L-HH|C-VV; (**c**) X-HH|X-HV|L-HH (Eckardt et al. 2013). The radar scenes are being used as an additional source of spectral information to overcome the problem of missing data due to cloud cover

wall products from radar backscatter retrievals using "hyper-temporal" statistics, a term introduced for radar applications by Schmullius and Santoro in 2007.

One of the first hyper-temporal retrievals for land cover applications had been performed with a non-imaging system, the wind scatterometer on-board ERS-1 for northern Eurasia (Schmullius 1997). Two indices had been introduced: the Slope Index (representing the incidence angle dependence of daily scatterometer measurements collected over 3 years), and the Radar Backscatter Index (RBSI) (defined as the ratio of the mean backscatter from large incidence angles over the absolute Slope Index). The RBSI is a measure of the amount of volume scattering from vegetation and showed – despite the very coarse resolution of 50 km – convincing correlations to the full range of canopy densities (best $r = 0.93$ for July). The RBSI correlation coefficients were investigated month by month and showed a relatively stable behaviour over the year (see Fig. 16.4). The dense time series revealed – for the first time – spatio-temporal pattern of freeze/thaw-processes, and secondly, an unexpected correspondence between 5-day interval backscatter time series anomalies with crop yield estimates for the former Soviet wheat belt.

About 10 years later, the hyper-temporal approach was extended to ScanSAR radar imagery: stacks of hyper-temporal ASAR Wide-Swath data led to a new retrieval approach – the BIOMASAR algorithm (Santoro et al. 2011). The algorithm is based on the famous Water Cloud Model (Attema and Ulaby 1978) and its extension to interferometry (Askne et al. 1997; Santoro et al. 2002). Collecting a minimum of 60 individual backscatter acquisitions per location, the typical radar noise is strongly reduced and a systematic sensitivity with even high forest densities and thus forest growing stock volume (GSV) was found. This finding was of special interest because C-band backscatter and coherence data were regarded to saturate at low biomass levels (Balzter et al. 2002; Balzter and Schmullius 2001; Luckmann et al. 2004; Schmullius et al. 2001; Wagner et al. 2003). Furthermore, the BIOMASAR algorithm does not require in-situ reference data for model training and completely relies on statistical estimates from backscatter data of unvegetated areas versus dense forest plots. These can be found by using other canopy products, e.g. MODIS Vegetation Continuous Fields (VCF). Validation showed that the approach is performing very well and is comparable to conventional approaches involving in-situ data for model training. No signal saturation is observed up to a GSV level of 300 m^3/ha and the relative root mean square error (RMSE) was between 34.2 and 48.1 % at a 1 km pixel size and consistently between 20 and 30 % at an 0.5° resolution as used by global vegetation models (Santoro et al. 2011, 2013a).

16.2.3 Time Series for Choosing the Right Scene(s)

Radar time series can also be used to select images of the most appropriate day-of-year, season or temporal combination for a specific application. For example, ASAR C-band time series were analysed as part of the ESA GMES (Global

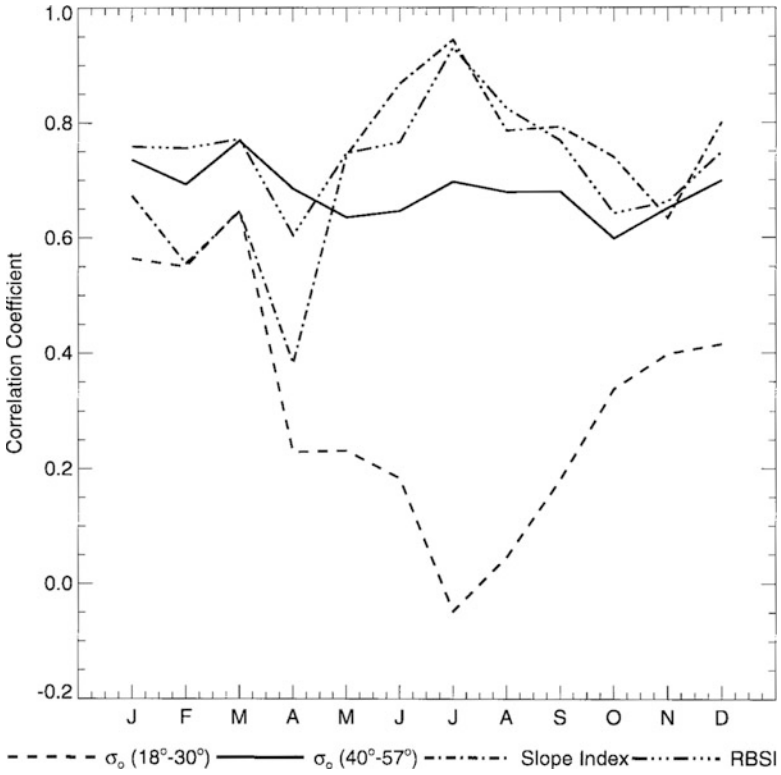

Fig. 16.4 Time series of correlation coefficients for four ERS-1 wind scatterometer parameters with canopy densities at 20 meteorological stations in Siberia (Schmullius 1997): normalised backscatter intensities at steep and large incidence angles, the slope of the incidence angle dependencies per month, and the Radar Backscatter Index (explained in the text). Values are monthly, three year averages (1992–1994). Canopy densities range from 5 to 90 %, the RBSI has a dynamic range from 4 to 12

Monitoring for Environment and Security) Service Element (GSE) Project "Forest Monitoring" with the unexpected result that April-scenes outperformed any other month to map forest disturbances in the boreal zone due to the specific scattering processes during the thawing period (Thiel et al. 2007, 2008). Ackermann (2015) investigated a total of 222 radar satellite scenes from TerraSAR-X, Cosmo-SkyMed (Constellation of small Satellites for Mediterranean basin Observation) and PALSAR (Phased Array type L-band Synthetic Aperture Radar) of a Thuringian forest site with an extensive set of ground data to quantify the impact of forest structure and temporal influences. Figure 16.5 shows one of the evaluated X-band time series, which can be summarized as temporally stable except major precipitation events leading to an increase. The time series also reveal an unexpected stability of the difference between spruce and beech forests – regardless of the chosen co-polarization HH or VV- even in winter times under leafless conditions.

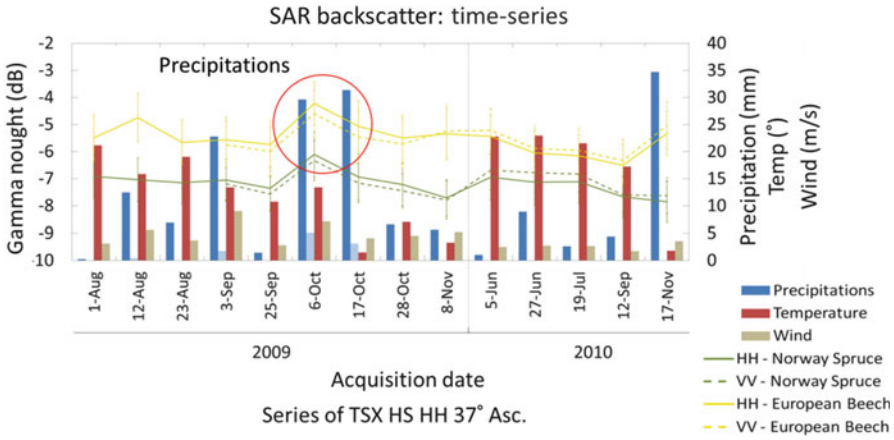

Fig. 16.5 TerraSAR-X backscatter time series over Thuringian forest test site. The signal stability demonstrates the all-year capabilities of X-band data for species discrimination between spruce needleleaf and beech broadleaf canopies (Ackermann et al. 2010). Major precipitation events increase overall backscatter (*red circle*), but separability is maintained

L-band backscatter intensities are strongly impacted by meteorological influences on the land surface conditions due to its much longer wavelength and thus deeper penetration into the canopy and, partly, into the upper soil layer. Moisture changes and particularly freezing events alter the scattering process significantly (compare Fig. 16.6). However, L-band coherence (coherence is the measure of phase correlation between two radar acquisitions) had revealed a large sensitivity and dynamic range to forest biomass (see Fig. 16.7). Coherence from winter showed a clear correlation with forest GSV. For summer scenes, the spread in the values was too large to give reliable results (Eriksson et al. 2003). Therefore, Eriksson et al. (2005) evaluated coherence from eight 44-day image pairs acquired with the Japanese Earth Resources Satellite 1 (JERS-1) during frozen winter conditions over several test sites in Siberia. A simple empirical exponential model was used for the retrieval. The results showed that under frozen winter conditions L-band repeat-pass coherence is a useful data source for stem volume retrieval, although accuracy decreases for higher stem volumes. The lowest retrieval error was 59 m^3/ha and with one exception the relative RMSE stayed within the range 42–76 %.

With increasing availability of L-band coherence time series from JERS-1 (1992–1998) and PALSAR on-board ALOS-1 (2006–2011) and -2 (launch 2014) a systematic investigation of the signal stability and influencing factors became feasible to support selection of best scenes for forest retrievals. Thiel and Schmullius extensively published on the retrieval performance under varying environmental conditions, which is described in the following illustrations:

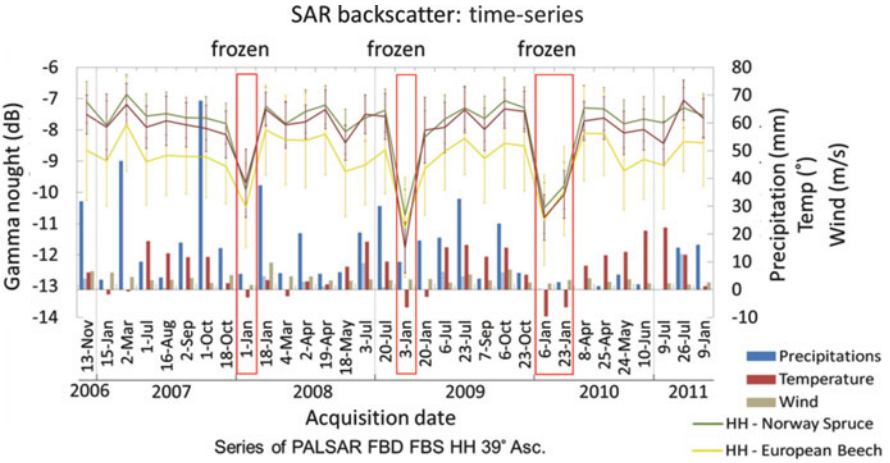

Fig. 16.6 PALSAR L-band time series from Thuringian forest test site exhibit very strong dependency on frozen conditions due to attenuation (Ackermann 2015)

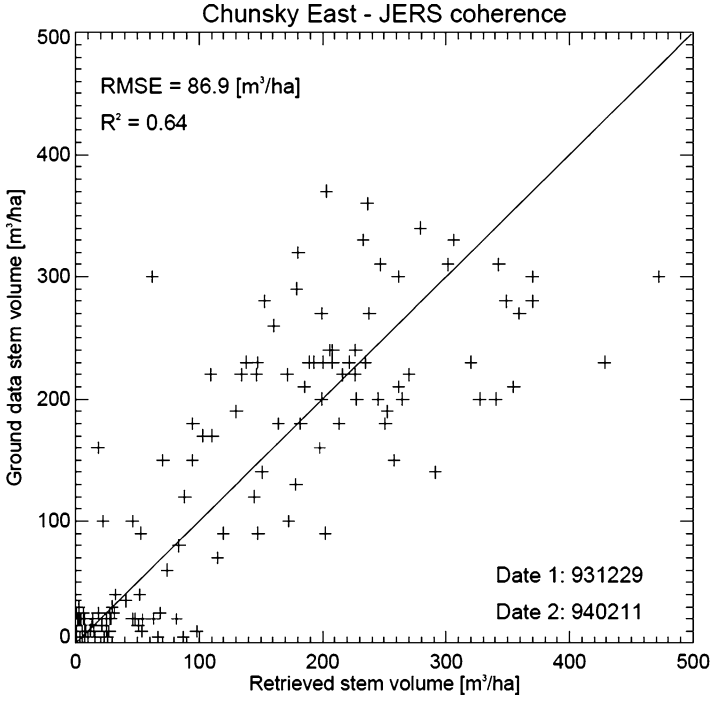

Fig. 16.7 Stem volume retrieval for the Siberian forest test site Chunsky East, Krasnoyarsk Kray. This result belongs to the first large-area application of an inversion model applied to L-band winter coherence values over a 1 mio km^2 forest area between Lake Baikal and the river Yenisei (Eriksson et al. 2005). This region represents commercially valuable forest stands that experience increased logging activities (compare Sect. 16.3.2, ZAPÁS Study)

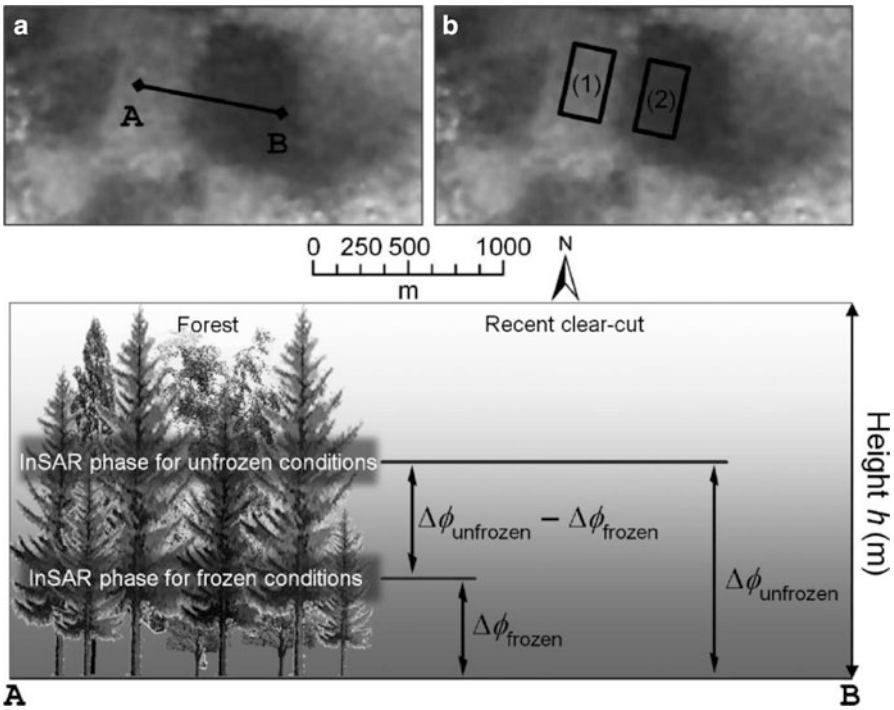

Fig. 16.8 PALSAR interferometric phase image from Chunsky test site in Siberia (57°49′12″ N, 97°2′48″ E). Bright areas are forest-covered, dark areas feature clear-cuts. (**a**) *A–B* defines the used transect and (**b**) shows the selected areas for phase calculation. The *bottom* graphic illustrates the location of the phase heights under unfrozen and frozen conditions. The difference in height amounts to approximately 4 m (Thiel and Schmullius 2013a)

Figure 16.8 – a phase height difference from unfrozen (8 m above ground) to frozen conditions (4 m above ground) has been determined from over 370 samples and 36 interferometric pairs (2013a),

Figure 16.9 – species-specific seasonal coherence behaviour was discovered and quantified (2014),

Figure 16.10 – effects of season and perpendicular and temporal baselines were summarized (2013b).

During frozen conditions an increased coherence over open areas was observed, decreased coherence over dense forest, decreased spread of coherence, and an improved correlation between |γ| and GSV. Furthermore, no indication was found that the perpendicular baseline impacted coherence levels from dense forest, whereas a difference was observed at unfrozen conditions. Consequently, at frozen conditions temporal decorrelation is the major source for diminishing coherence values of up to 0.3 points. Hence, |γ| acquired under frozen conditions has good and consistent potential for GSV mapping. The relationship between GSV and |γ| was

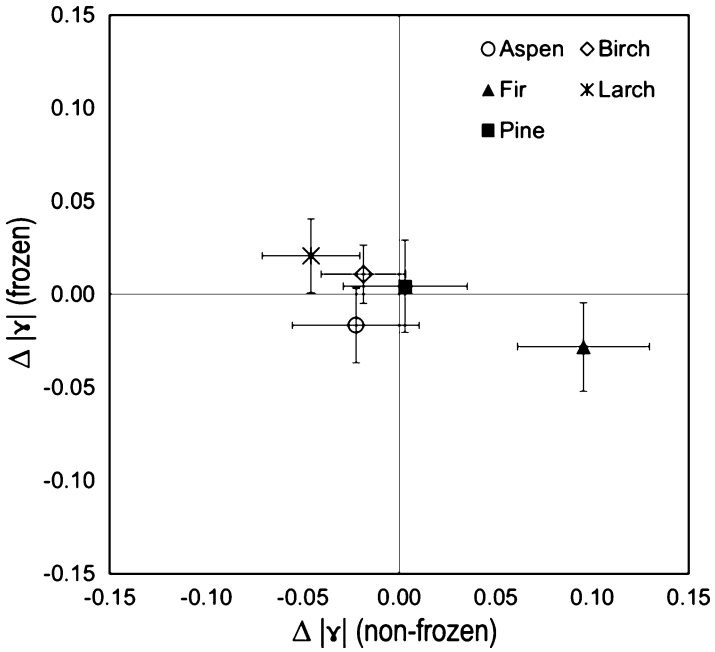

Fig. 16.9 Deviation Δ of species-specific coherences γ from average coherence values for dense forests under frozen and non-frozen conditions for all sites (11 forest enterprises with a total of 12,243 stands covering 3,097 km^2). Frozen conditions exhibit species-independent stable coherence values, whereas intra-species variance and species-dependency increases for non-frozen states (Thiel and Schmullius 2014)

found to have an average coefficient of determination R^2 of 0.6. Saturation occurs at about 250 m^3/ha.

16.3 Case Studies

The results presented in Sect. 16.2 refer to discoveries and manifestations that have already proven their operational character for land or forest cover monitoring for large-area mapping – either through the sheer size of the investigated region or the extremely large number of temporal data stacks. In this section, we present state-of-the-art case studies which have not been tested in space or time for their operationality, but that are ready for a proof-of-concept.

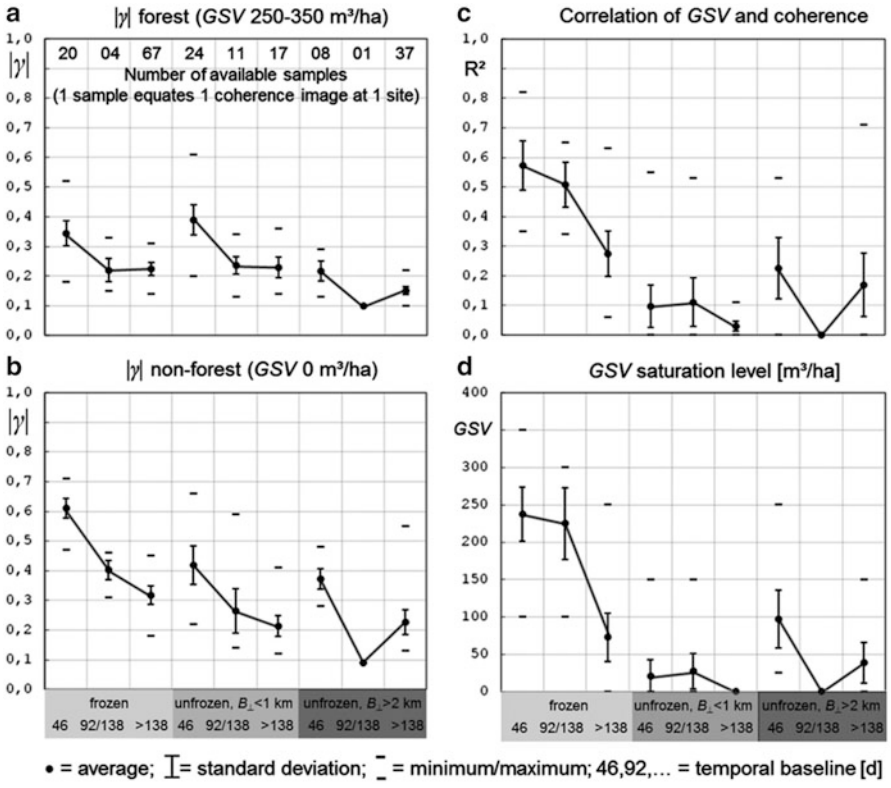

Fig. 16.10 Summary of coherence characteristics based on 300 interferograms from ALOS-1 PALSAR data and 12,243 forest stands in central Siberia (Thiel and Schmullius 2013b): (**a**) |γ| for forest, (**b**) |γ| for non-forest, (**c**) correlation coefficient for GSV and |γ|, and (**d**) saturation level for GSV. All graphs are separated into three columns for frozen and six columns for unfrozen conditions; unfrozen conditions are further divided into perpendicular baselines <1 km and >2 km. Each of the three groups has one column representing a temporal Baseline of 46 days, one for either 92 or 138 days, and one for more than 138 days. See the *first row* in (**a**) for the number of available samples for each of the nine columns

16.3.1 Land Cover Classification Using Multi-temporal C-Band Data

Sentinel-1, the new European radar satellite launched on 3rd April 2014, represents the start of ESA's third decade of continuous C-band sensors in space: ERS-1 and-2 since 1991 and 1995 respectively, and ENVISAT ASAR from 2002 to 2012. Compared to its predecessors, Sentinel-1 provides much shorter revisit times of only 12 days and an increased geometric resolution of 10 m in its Interferometric Wide-Swath Mode. These improved specifications represent an increased potential for operational land cover products. Two ESA studies which specifically focussed on the benefits of radar time series for land cover mapping to prepare the

operational use of Sentinel-1 are presented in this section: AMOC-I (Acoustic Monitoring of the Ocean Climate) (Cartus et al. 2008), and AMOC-II (Thiel 2010). Mapping approaches based on radar data need to consider the issue of speckle respectively radiometric accuracy. For mono-temporal intensity images, speckle reduction can only be achieved by using filters that reconstruct the local radar cross section by means of spatial averaging causing a loss of geometric resolution. For time series, Quegan and Yu (2001) suggested a multi-temporal filtering approach, eventually leading to multi-temporal statistics. For the classification of five basic (Level 1) land cover classes, i.e. Water, Forest, Settlement, Grassland and Agriculture, Cartus et al. (2008) analysed four multi-temporal metrics characterising the temporal variation of SAR backscatter:

- minimum / maximum / mean backscatter for each pixel in all images,
- mean annual variation (MVA).

MVA can be calculated as follows (Quegan et al. 2000):

$$mva = 10 \cdot \log\left[\frac{2}{N(N-1)}\sum_{i=1}^{N-1}\sum_{j>i} R_{ji}\right] \quad R_{ij} = \max\left({}^{I_i}/_{I_j}, {}^{I_j}/_{I_i}\right) \tag{16.1}$$

where N represents the number of images and R the normalized ratio of intensities. When calculating the MVA for the speckle filtered VV, HH and HV polarised data, a clear difference between agricultural areas and the land cover classes forest, settlement and grassland was found. This difference was most pronounced for the HV data (Fig. 16.11).

Figure 16.12 shows histograms of the four multi-temporal metrics. The MVA generally reflects the high temporal stability of backscatter over forest, settlements and grassland. The best contrast between these classes and agricultural areas is found using the HV polarization. Forest has an MVA <1 dB in the co-polarised and <2 dB in the cross-polarised images. Settlements show very stable backscatter, but for some dense built-up areas the MVA is high because of different ascending and descending viewing directions (Henderson and Lewis 1998: p. 741). The very low HV backscatter allows a simple discrimination of water from other classes. Differentiation of forest and grassland is not possible using the MVA, but using the annual mean, maximum and minimum backscatter in all three polarisations. Differentiation of forest and settlement seems not to be possible based on multi-temporal metrics. Thus, textural measures are needed.

The analysis of the multi-temporal statistics resulted in a procedure, which classifies C-band data reliably into five Level-1 land cover classes by innovatively using multi-temporal metrics instead of using only backscatter intensities (see Fig. 16.13). Thinning studies about the amount of input data showed that the requested overall accuracy of 85 % and individual class accuracies of at least 70 % can be reached when a minimum of four C-band acquisitions during the growing season are available with HH/HV- or VV/VH-polarisations (Thiel et al. 2009c). ESA's Sentinel-1 satellite now consistently provides the required

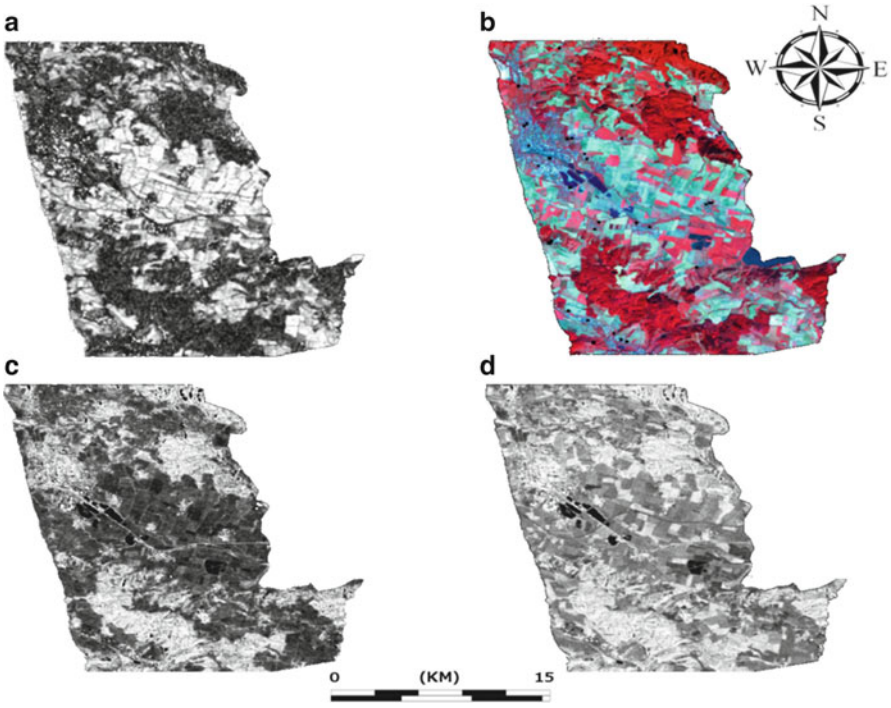

Fig. 16.11 Multi-temporal metrics of 14 ASAR AP HV polarimetric intensity images with (**a**) MVA (explanation in text), (**c**) annual minimum σ^0, (**d**) annual mean σ^0. (**b**) shows for comparison a Landsat ETM+ NIR-Red-Blue RGB-colour composite acquired Sep. 4th 1999 (Cartus et al. 2008). The geographical area is the same as in Figs. 16.2 and 16.3 with UL coordinates 53°33′N/10°44′E, and LR 51°22′N/11°02′E

dual polarisation C-band measurements with short revisit times. These data sets could be used stand-alone for operational land cover mapping as shown in Fig. 16.14.

The results presented in Sect. 16.2 refer to discoveries and manifestations that have already proven their operational character for land or forest cover monitoring for large-area mapping – either through the sheer size of the investigated region or the extremely large number of temporal data stacks. In this section, we present state-of-the-art case studies which have not been tested in space or time for their operationality, but that are ready for a proof-of-concept.

16.3.2 Forest Mapping Using Radar Time Series

Until multi-temporal C-band backscatter intensity and coherence acquisitions became available, forest mapping capabilities were assigned to L-band data or

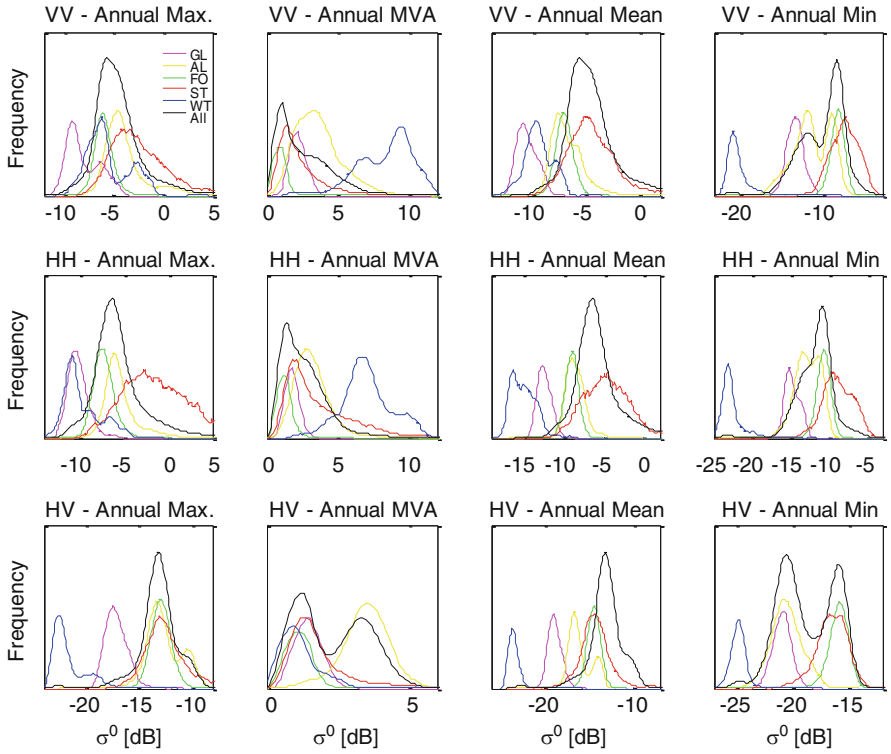

Fig. 16.12 Histograms of multi-temporal metrics for land cover classes Grassland 'GL' (magenta), Agriculture 'AL' (*yellow*), Forest 'FO' (*green*), Settlement 'ST' (*red*), and Water 'WT' (*blue*) (Cartus et al. 2008)

even longer wavelengths (e.g. Dobson et al. 1992). Therefore, interpretation of 1-day repeat-pass "Tandem" coherence images from ESA's ERS-1 and -2 satellites in the late 1990s showed surprising results with stable correlations to forest density – a feature which was then extensively applied for the first 1 million km^2 radar-retrieved biomass map of Siberian forests (Schmullius and Rosenqvist 1997b; Schmullius et al. 2001). A further discovery followed about 10 years later with the availability of "hyper-temporal" C-band Wide-Swath and Global ScanSAR Mode time series from ESA's ASAR sensor on-board ENVISAT: the sensitivity to GSV could be increased to over 300 m^3/ha (Santoro and Cartus 2010).

Two case studies are hence described in this section: the application of the former SIBERIA algorithm to forest mapping in China in the framework of the ESA DRAGON-1 program (http://earth.esa.int/dragon/); and secondly, the production of the first radar-retrieved continuous GSV map of the Northern Hemisphere based on the BIOMASAR-algorithm (http://biomasar.org/).

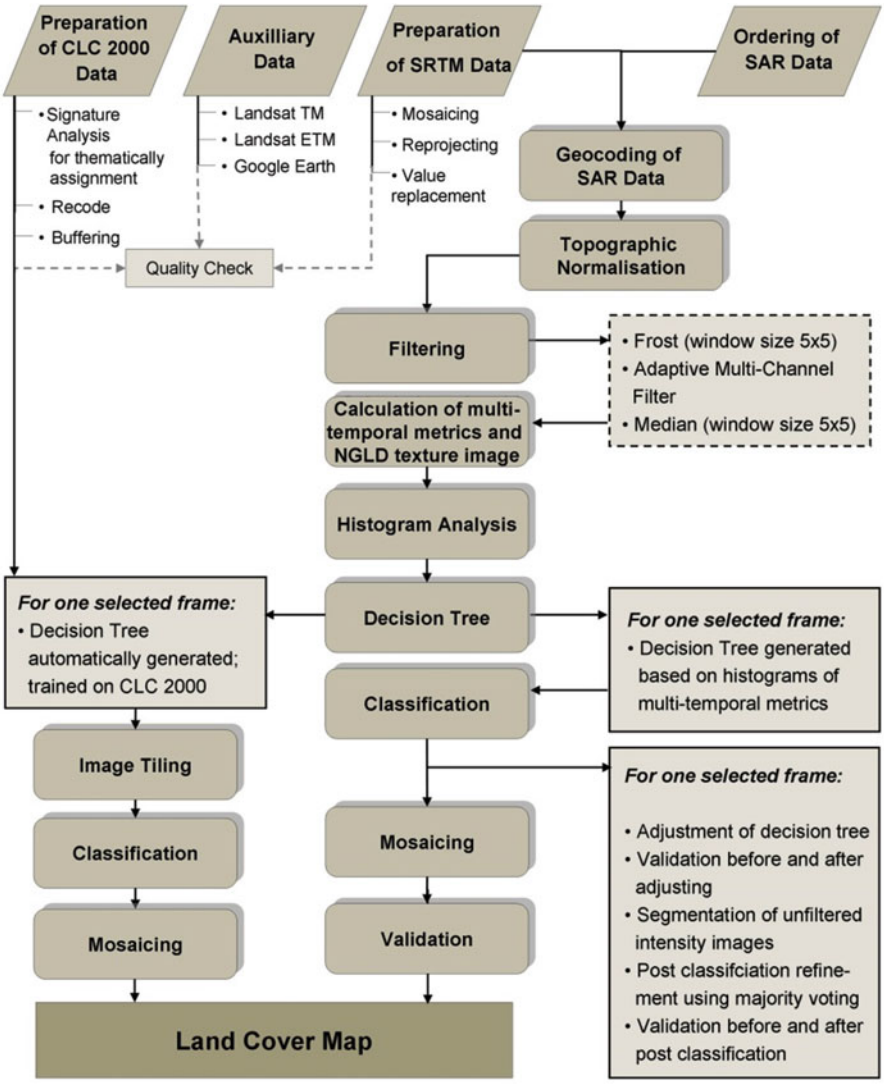

Fig. 16.13 SAR pre-processing and classification chain in ESA AMOC II Study to prepare operational use of Sentinel-1 data for land cover mapping (Thiel 2010). The resulting land cover map of this procedure is illustrated in Fig. 16.14

16.3.2.1 DRAGON-1 Case Study

ERS-1 and -2 Tandem coherence has high potential for mapping boreal forest stem volume (e.g. Askne and Santoro 2005). Large-scale application, however, is hindered by the variability of coherence with meteorological and environmental conditions. Retrieval procedures therefore need to be based on model training

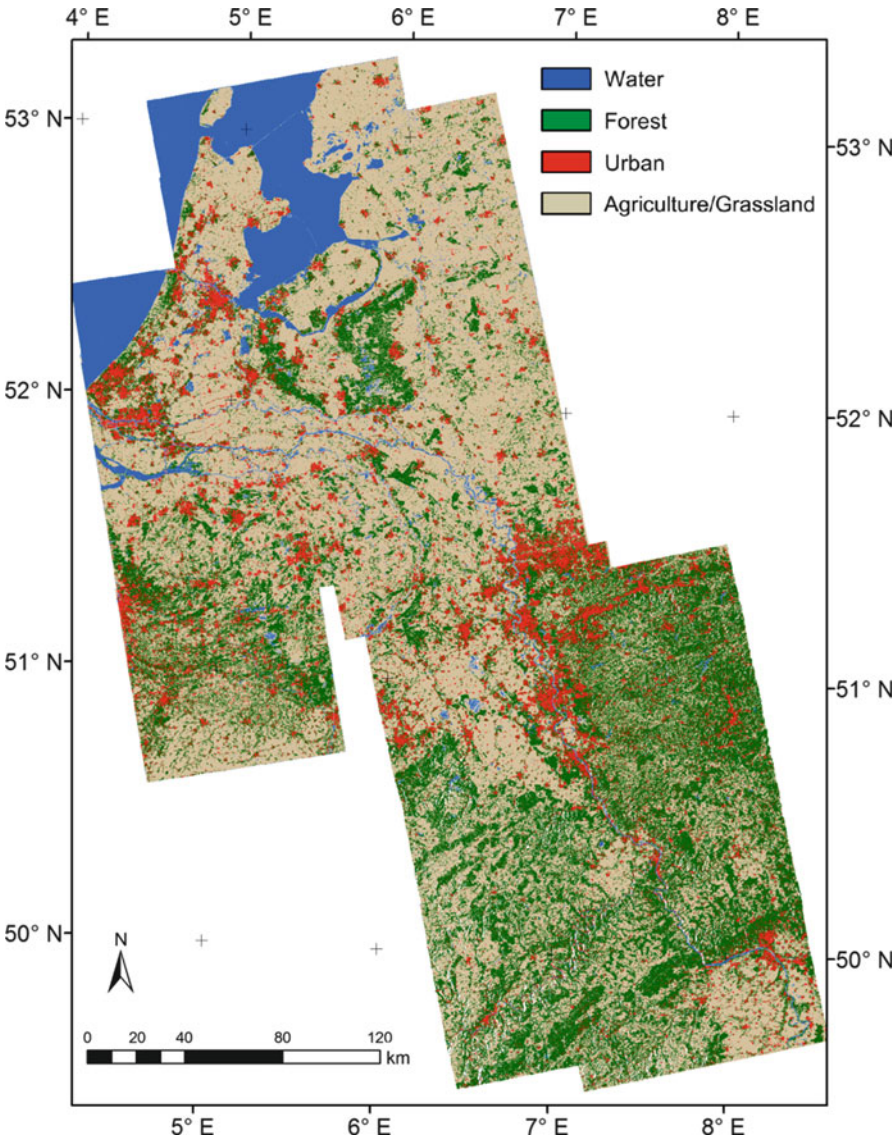

Fig. 16.14 In order to generate a large land cover map of ca. 75,000 km^2 from SAR data (covering parts of the Netherlands, Belgium and Germany), a knowledge-based decision tree has been applied to 11 Envisat ASAR frames without any local adjustment. The incidence angles vary between modes IS 1 and IS 3. The classification procedure is based on backscatter intensity, multi-temporal metrics and texture features. The map was validated using 50 geo-referenced Quick Bird snapshots with 496 reference points. The overall accuracy of the complete land cover map (with a merged class containing grassland and agriculture, as originally intended by ESA) was found to be 89.72 % (Thiel 2010)

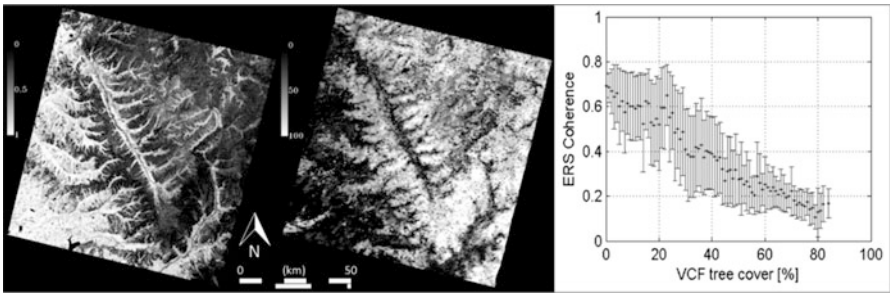

Fig. 16.15 ERS-1/-2 Tandem coherence (*left*) and VCF tree cover (*middle*) for a forested area in NE China. The coherence image is based on acquisitions from 3./4. Oct 1997. The *right* plot shows the decrease of coherence with increasing VCF tree cover ±1 standard deviation. VCF values end at 80 % cover, hence higher density and biomass classes cannot be trained without inventory information (Cartus et al. 2011)

relating coherence to stem volume by using forest inventory data, which is generally only available for a few small test sites. In the Forest-DRAGON project, a new approach was developed that allows model training based on the MODIS Vegetation Continuous Fields canopy cover product (Hansen et al. 2003) without further need for in situ information. A comparison is shown in Fig. 16.15.

As a test for wall-to-wall nation-wide applications, the retrieval method was applied to a multi-seasonal Tandem dataset consisting of 223 ERS-1/-2 image pairs covering northeast China (~1.5 million km^2). The coverage is shown in Fig. 16.16. Four stem volume classes were produced (0–20, 20–50, 50–80, and >80 m^3/ha). The agreement in terms of the kappa coefficient was between $\kappa = 0.52$–0.87 with a standard deviation of 20 m^3/ha. For images acquired in winter, κ was between 0.71 and 0.87; for images acquired in fall and spring it was between 0.52 and 0.78. The producer and user accuracies of the intermediate volume classes reached >80 %. Hence, a regression-based retrieval for forest stock discrimination with ERS-1/-2 Tandem coherence and the VCF-based model training approach appears justified.

16.3.2.2 BIOMASAR Case Study

Promising results from a hyper-temporal retrieval experiment concerning biomass mapping for Sweden, Quebec and central Siberia by Santoro and Cartus (2010) led to an unprecedented endeavor employing more than 647,000 ASAR ScanSAR C-band backscatter data sets acquired between October 2009 and February 2011 over the North American and Eurasian continent: the production of the BIOMASAR forest GSV map of the Northern Hemisphere (Santoro et al. 2013b). Figure 16.17 gives an impression of the hyper-temporal data quantity. The innovative aspect of the algorithm is its independence from in situ measurements for model training. Model parameter estimates are obtained from tendency statistics of

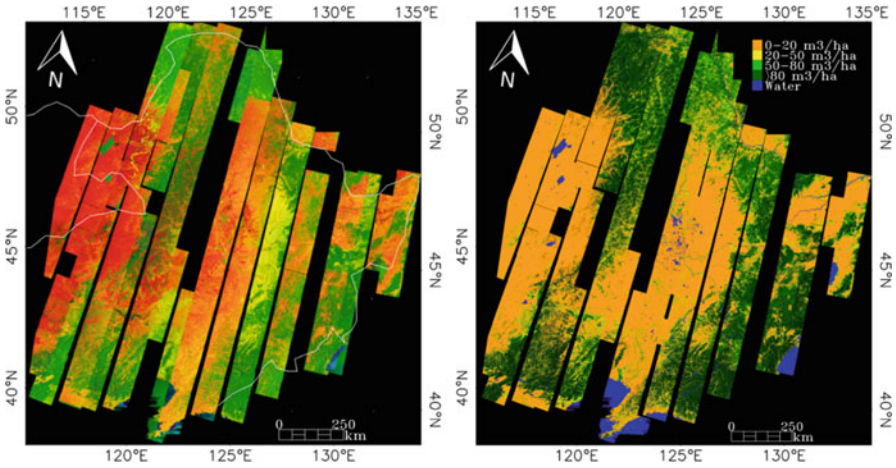

Fig. 16.16 *Left*: Mosaicked ERS-1/-2 false-color composite of northeast China: R-Tandem coherence, G-ERS-1 intensity, B-ERS-1/-2 intensity difference. The mosaic consists of 223 frames with 50×50 m^2 pixel size. Color differences between different tracks are caused by environmental effects. *Right*: Mosaic of the classified GSV maps from ERS-1/-2 Tandem data. The adaptive retrieval model has effectively removed the differences in the input data (Cartus et al. 2011)

the backscatter measurements for unvegetated and dense forest areas, which can be selected using a continuous tree canopy cover product, such as MODIS VCF.

Data processing included multi-looking to 1 km pixel size, terrain geocoding to a pixel size of 0.01°, speckle filtering and correction for slope-induced effects on the backscatter. Validation of the GSV maps was carried out at the full resolution of 0.01° as well as at the aggregated level by comparing against in situ and optically-based official inventory information. Detailed validation at the full 1 km resolution with the Swedish, Quebecan and central Siberian forest inventories proved consistent GSV estimates with a good agreement up to 300 m^3/ha and an underestimation of GSV for biomass levels above 300 m^3/ha. Overall, the RMSE is between 28.7±10.0 % at 1 km pixel size (Santoro et al. 2015). Larger errors were obtained at 100 m spatial resolution because of local errors in the reference datasets. Averaging GSV estimates over neighboring pixels improved the retrieval statistics substantially. For an aggregation factor of 10×10 pixels, the relative RMSE was below 25 %. In general, the spatial patterns of the estimated SAR-based GSV showed good agreement with those of existing reference data sets at a similar spatial resolution. The resulting BIOMASAR map is shown in Fig. 16.18.

16.3.3 Forest Cover Change with Radar Time Series

Forest cover monitoring requires regular observations throughout the year, depending on the biome and the respective fire and/or logging activities. The

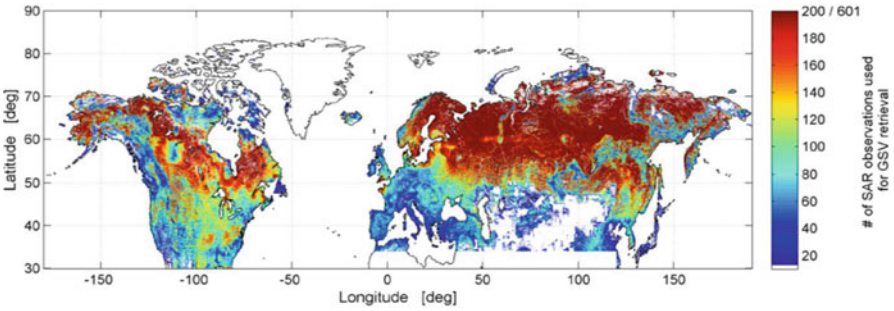

Fig. 16.17 Number of SAR observations used for the Growing Stock Volume (GSV) retrieval. The color bar is constrained between 10 and 200, while the number of observations reached up to 601. Zero is assigned to unmapped pixel and pixels for which the number of SAR observations was less than 10, i.e. represent unreliable estimates for the retrieval model (Santoro et al. 2013b)

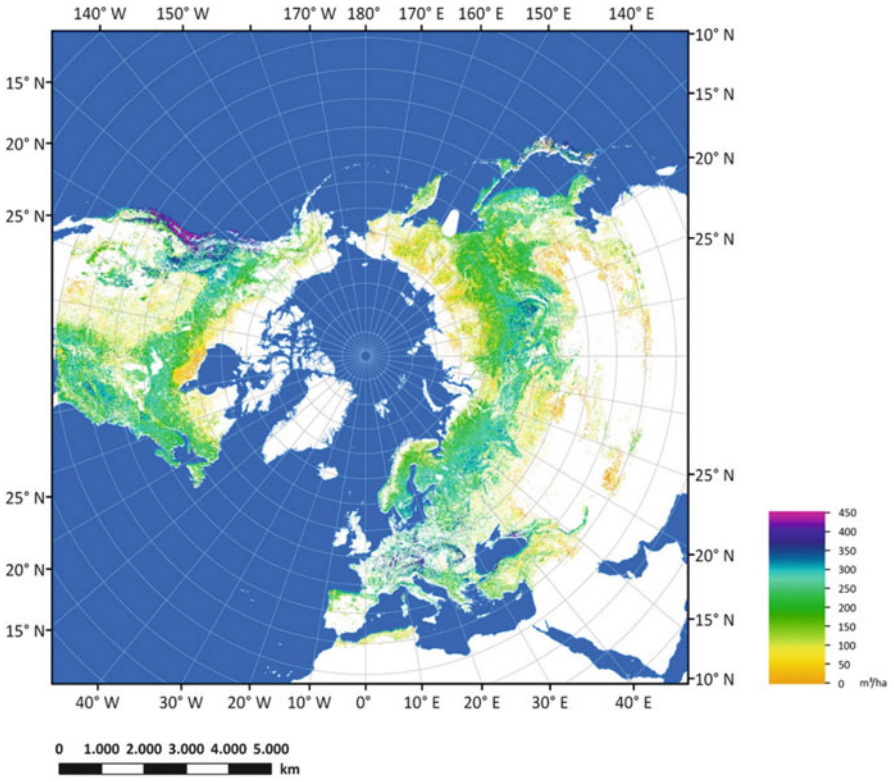

Fig. 16.18 The BIOMASAR Growing Stock Volume (GSV) Map from ENVISAT, www.esa.int/Our_Activities/Observing_the_Earth. The color bar is constrained between 0.1 and 450 m^3/ha, while the retrieved GSV reached up to 1,019 m^3/ha (Santoro et al. 2013a)

Japanese space agency Japan Aerospace Exploration Agency (JAXA) has been the only SAR data provider offering a consistent observation strategy based on the recommendations of its Kyoto and Carbon Panel for more than two decades since its first radar sensor JERS-1 (e.g. Rosenqvist et al. 2007). These L-band data sets reveal less temporal decorrelation when calculating interferometric coherence due to the longer wavelength and thus larger and more stable scattering elements. Hence, multi-temporal coherence and multi-temporal backscatter intensity can both be exploited to build an operational change procedure, as demonstrated by Thiel et al. (2009a, b) where ALOS-1 PALSAR summer intensities and winter coherences led to segment-based classification accuracies of 93 % for a 100,000 km^2 study area for seven classes: water, urban, arable, burnt, recent and old clear-cuts.

The following two case studies extend the application of radar remote sensing to multiple satellites. The first study describes how three radar time series products have been jointly exploited to map forest cover change – independently of the fact that they have been generated from different sensors (ERS-1/-2 vs. ASAR) and different algorithms (SIBERIA vs. BIOMASAR). The two respective methods were described in Sect. 16.3.2. The second study comprises a joint usage of the PALSAR mosaic time series with the multi-temporal MODIS Enhanced Vegetation Index to increase the reliability of disturbance mapping.

16.3.3.1 DRAGON-2 Case Study: Merging Space and Time

The forest project contributing to the second ESA cooperation program with China, DRAGON-2 (https://saredu.dlr.de), focused on the evaluation of multi-temporal, multi-sensor and multi-scale Earth Observation products of northeastern China. First, the GSV map produced with ERS-1/-2 coherence images for 1995–1998 using the SIBERA-algorithm (Fig. 16.16) and the GSV map produced from Envisat ASAR ScanSAR data from 2007 to 2008 with the BIOMASAR-algorithm (Fig. 16.19) were compared with several land cover/forest cover products of optical origin. These comparisons were used to assess the plausibility of the respective GSV estimates to undertake the change study. The change analysis was carried out in the regions of Daxinganling (~200 × 200 km) and Xiaoxinganling (~300 × 300 km) in northeast China.

Leiterer et al. (2010) developed a multi-scale cross-comparison assessment design that uses few in situ measurements and data quality flags and applies existing land cover products such as GlobCover, MODIS VCF, GLC2000 (Global Land Cover (GLC2000)) and the AVHRR LCC(Lambert conic conformal). The sampling design for the comparison is based on the FAO (Food and Agriculture Organization) Forest Resource Assessment 2010, which uses a 1° sampling grid with 10 × 10 km sample plots. The results are shown in Table 16.1. Additionally, forest GSV inventory data including >1,100 point measurements were available for a small test site in northeast China showing good overall accuracy of 76 % for the ERS-retrieved map.

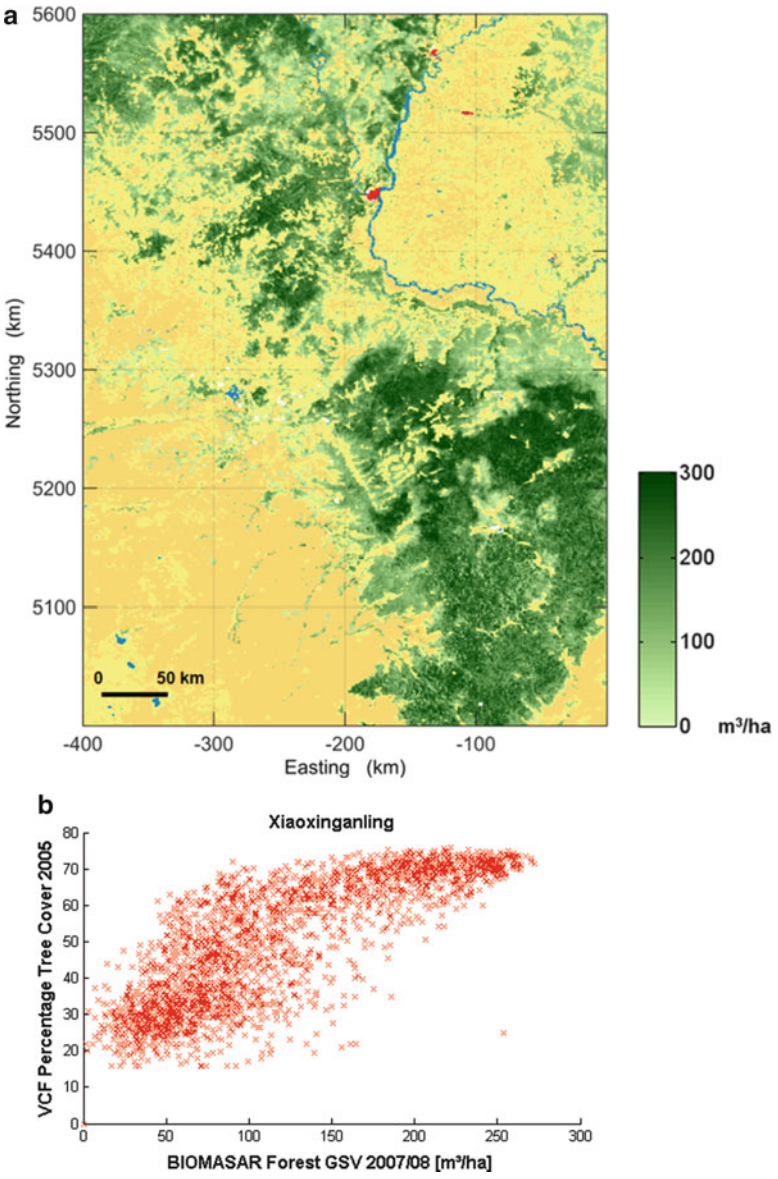

Fig. 16.19 (**a**) ASAR-retrieved GSV map 2007/2008 (pixel size 1 km) illustrating great amount of heterogeneity; green tones: forest GSV, other colours non-forest land cover types. (**b**) scattergram of ASAR GSV versus Vegetation Continuous Field percentages showing the known VCF-threshold at 80 % cover and that the ASAR-product has not reached saturation yet (Reiche et al. 2010)

Table 16.1 Overall agreement (OA) between ERS-1/-2 GSV map (50 m resolution, Fig. 16.16) and four optical land cover products for test areas 1-Daxinganling and 2-Xiaoxinganling in NE China based on aggregated forest/non-forest classes (Leiterer et al. 2010)

LC-product	Site 1	Site 2
NLCD	0.73	0.80
GlobCover	0.78	0.85
VCF (15 % CC)	0.91	0.89
GLC2000	0.89	0.83
AVHRR LCC	0.79	0.67

The Chinese national land cover product NLCD (National Land Cover Database) (based on Landsat images) identified that misclassification of the ERS-maps primarily took place at croplands. Thus, land cover information should be used to support the radar-retrievals particularly for transition zones between forest and shrub land. Cross-comparison for the ASAR forest maps revealed, that the spatial variability was more reliably captured (using NLCD as reference again) than with other land cover products. Figure 16.19a illustrates the heterogeneity of the forest cover in the Xiaoxingaling test area as identified by the ASAR-retrieved GSV map and Fig. 16.19b) shows the scatterplot comparison with VCF tree cover percentages for the same area.

To undertake the forest change exercise, the ERS data were reprocessed to the coarser ASAR Global Monitoring Mode resolution of 1 km. The resulting change map is given in Fig. 16.20. It is the first 10-year forest stock change representation from multiple SAR-sensor time series and thus a milestone in radar remote sensing. Missing tracks are a result of missing ERS-Tandem acquisitions. Solely ASAR-based GSV estimates for the time period 2005–2010 are shown in Fig. 16.21 and have been checked for plausibility during field campaigns and using related Earth observation products (compare Fig. 16.22). Patterns of increase and decrease in that 5-year period can be explained with growth models and fire events respectively. However, a distributed geo-spatial error quantification could not be performed due to missing in situ information.

16.3.3.2 ZAPÁS Case Study – Operational Radar-Optical Synergy

Forest cover disturbance rates of Siberian forests are increasing due to intensification of human activities and changing climate conditions. Hüttich et al. (2014a) used a radar-optical data concept to develop an automated forest cover change detection: pre-classification change-detection techniques were applied to annual ALOS PALSAR backscatter mosaics (2007–2010, see Fig. 16.23) to assess yearly forest biomass loss; and time series of the MODIS Enhanced Vegetation Index product (EVI, 2000–2014) were integrated in a web-based middleware system to establish near-real time detection of forest disturbances using the Breaks For Additive Season and Trend (BFAST) method. Using the Earth Observation Monitor

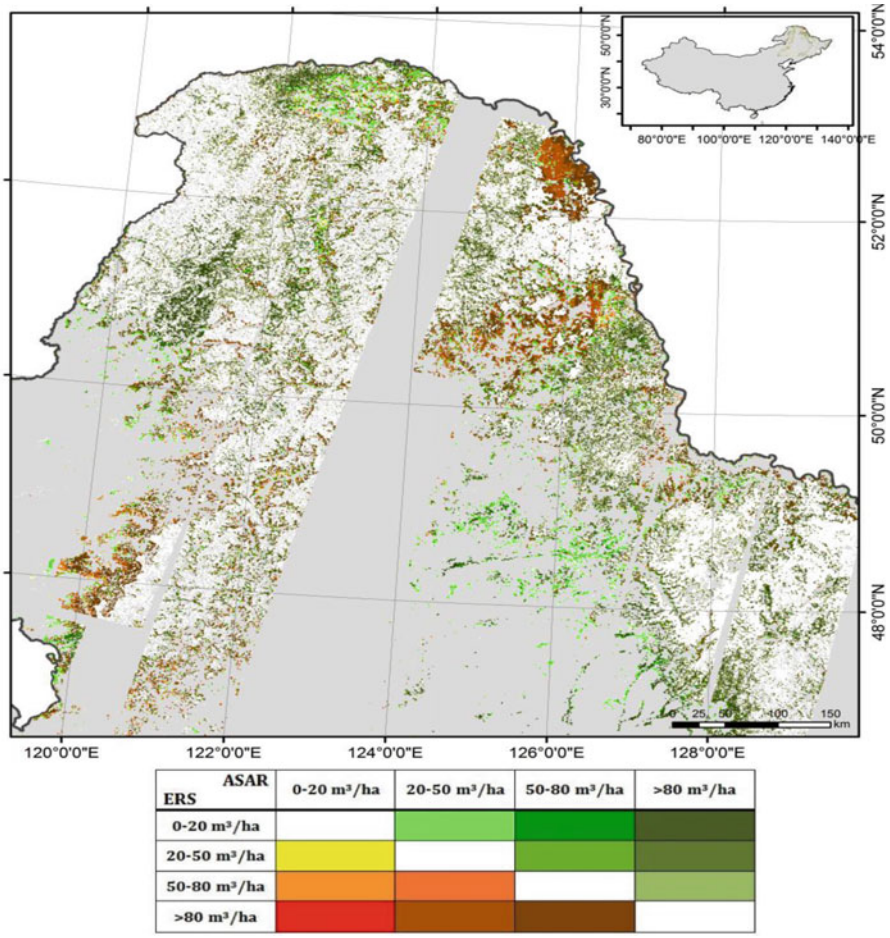

Fig. 16.20 Forest stock change of a ten year period is mapped in four Growing Stock Volume classes using an ERS Tandem dataset and a hyper-temporal ASAR image stack. The tandem product is based on the SIBERIA algorithm, the hyper-temporal method on the BIOMASAR retrieval method. The twelve change classes correctly identify in green colors areas of extensive re-forestation after very large forest fires in 1987; the brown regions indicate burnt zones as a result of a 2006 fire (Reiche et al. 2010). This map represents the first published growing stock volume change product from multiple radar sensors using different retrieval algorithms that combine interferometric with hyper-temporal techniques. The Tandem GSV product with a geometric resolution of 50 m was resampled for this purpose to the 1 km resolution of the ASAR hyper-temporal GSV product. (© FSU Jena, GAMMA RS)

(EOM, www.earth-observation-monitor.net) an operational monitoring system was assessed for the capabilities to detect biomass loss and to analyze temporal patterns of forest cover loss related to logging activities, fire events or other disturbances.

A pre-classification approach using a decision-tree classifier was implemented. Only changes from forest to non-forest were considered. In order to identify

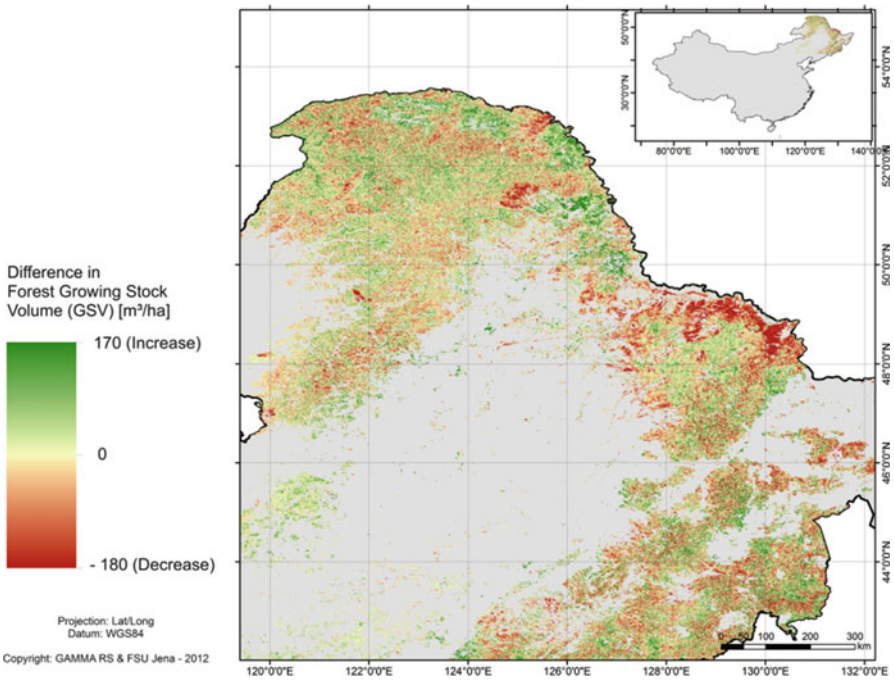

Fig. 16.21 Growing Stock Volume (GSV) change map from estimates obtained with the BIOMASAR algorithm using Envisat ASAR ScanSAR images acquired in 2005 and 2010 (Schmullius et al. 2012). The study area has a total coverage of about 540,000 km^2 including forest and shrubland areas according to the GLC2000 land cover information. The map is characterized by several changes through fire, logging and re-forestation. The GSV estimated with the BIOMASAR algorithm presents an uncertainty quantified on the order of 10 % regardless of the GSV level as proven with comparable inventory data from Siberia

common classification thresholds eight different multi-temporal metrics were analyzed (compare Fig. 16.24). The forest/non-forest change thresholds were detected using non-parametric support vector machines (SVM).

The PALSAR-based average accuracy of forest loss detection was 70 %, whereas the MODIS-based change assessment using breakpoint detection achieved average accuracies of 50 % for trend-based breakpoints and 43.4 % for season-based breakpoints. Time series tracking of phenological activities was realized using the MODIS EVI product with a 16-day temporal resolution for additional information on forest disturbances. Two years (2009 and 2010) showed higher user accuracies of 80.0 %. It is assumed that the PALSAR input mosaics for those years had been acquired under more stable radiometric conditions, which demonstrates the need for free access to raw data rather than processed data products. The sensor's 46-day revisit time is not a limitation due to the stable environmental conditions during winter (even for coherence estimates). This is of particular importance for the development of an operational large-scale forest-monitoring system for the boreal region: the mentioned accuracies are well in the range of

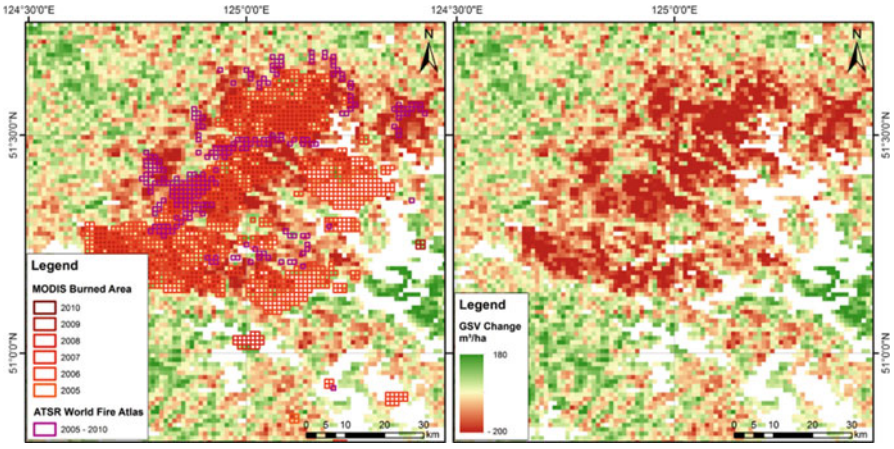

Fig. 16.22 MODIS Burned Area and ATSR World Fire Atlas overlaid on the GSV change map (*left*) and GSV change map (*right*) for a fire detected in 2006 showing very good agreement for the areas affected by stock volume losses. (Schmullius et al. 2012)

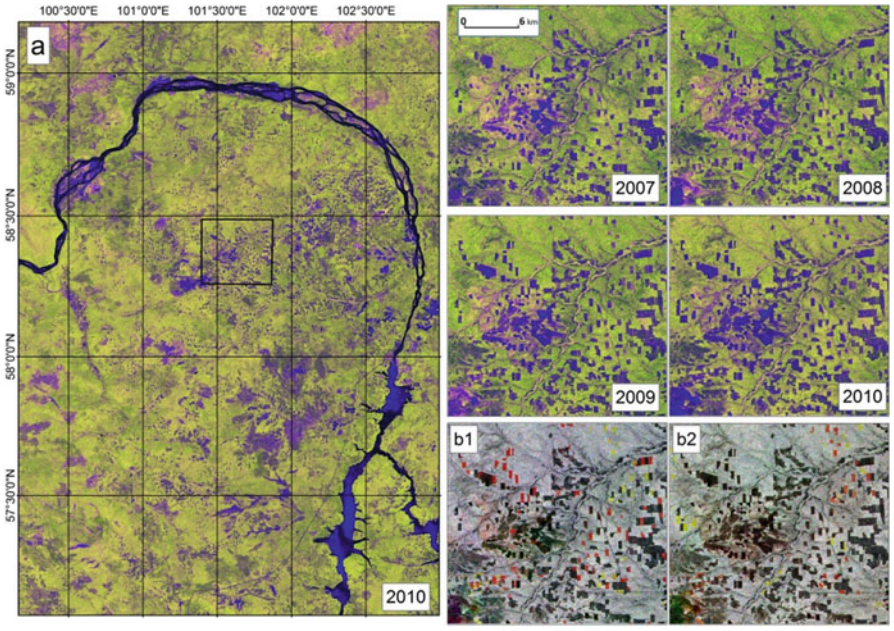

Fig. 16.23 False-color RGB composites of ALOS PALSAR 25 m mosaic images, acquisition periods each year May-October, and incidence angle 34.3°. (*a*) *Red*: HH-intensity, *Green*: HV-intensity, *Blue*: ratio HH/HV; same color scheme applies for zoomed area in 2007, 2008, 2009, and 2010 (Hüttich et al. 2014a, b). Change is shown for the zoom region as color composites with (*b1*) Red-2007, Green-2008, Blue-2009; and (*b2*) Red-2008, Green-2009, Blue-2010. The data were made available through the ALOS Kyoto and Carbon Initiative of JAXA

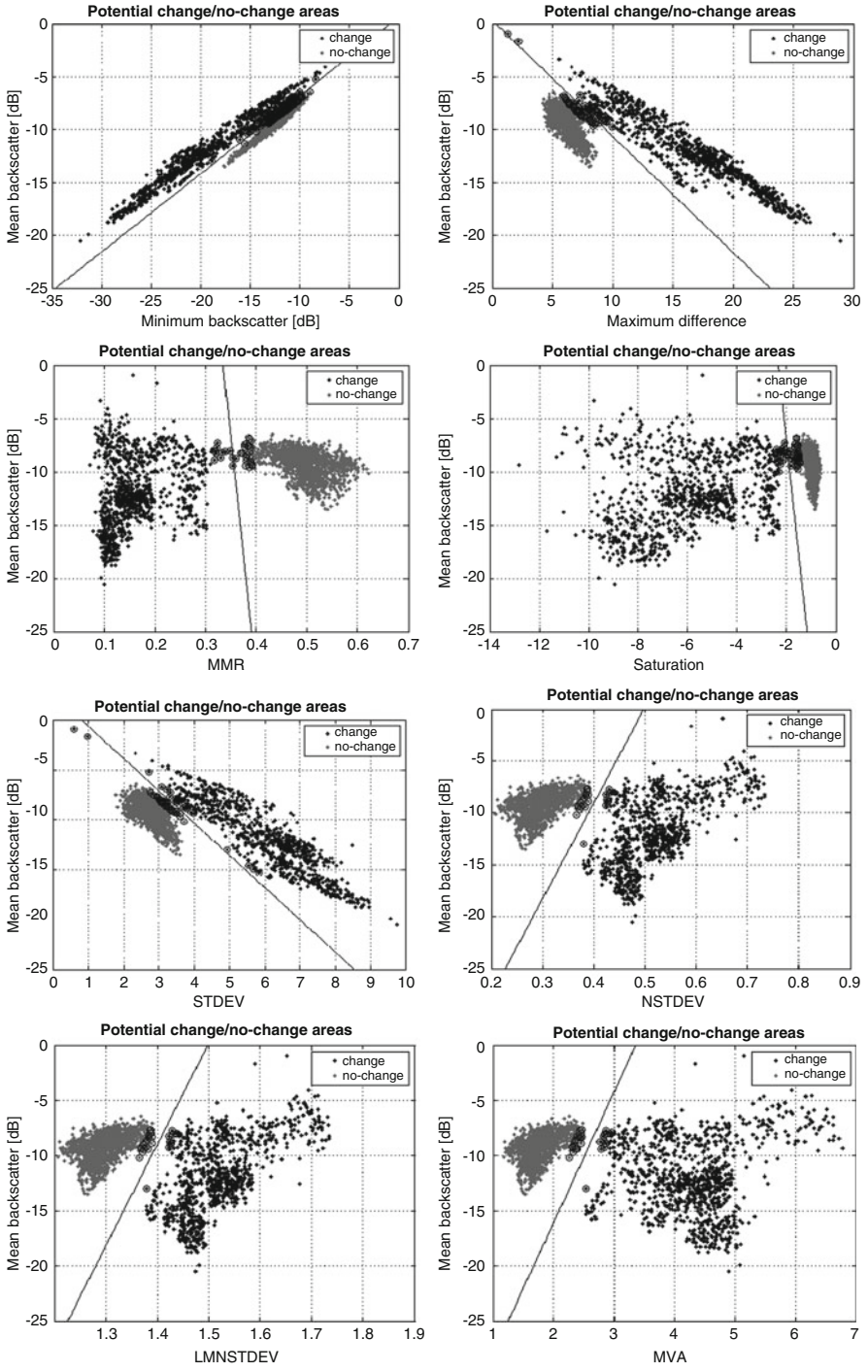

Fig. 16.24 Multi-temporal metrics to identify thresholds for forest change/no-change classification with PALSAR data: maximum-minimum ratio (MMR), normalized standard deviation (NSTDEV), mean average variability (MVA), and logarithmic measure based on normalized standard deviation (LMNSTDEV). The largest class separability was calculated for HV-polarization (Hüttich et al. 2014a, b)

inventory errors of 34–39 %, as has been investigated stand-wise in Hüttich et al. (2014b).

It can be concluded, that the freely available PALSAR mosaics are an applicable tool for up-to-date forest monitoring – even considering varying accuracies. Monitoring can be enhanced through web-based middleware exploiting MODIS time series and the BFAST-method to suggest the type of disturbance.

16.3.4 Special Seasonal Case: Savanna Systems

Woody vegetation cover affects a range of ecosystem processes such as carbon and water cycling, energy fluxes, and fire regimes. Information on the spatial distribution of woody vegetation over large areas is needed to understand the dynamics of savanna ecosystems. In this study, fractional woody cover was mapped using ALOS PALSAR L-band HH- and HV-polarised backscatter time series. The SAR backscatter intensity and two polarimetric decompositions were compared with woody cover obtained from high-resolution airborne LiDAR (Light detection and ranging) data using a semi-empirical exponential model. The SAR data were acquired at different seasonal cycles between 2007 and 2010. The LiDAR survey was carried out in April/May 2008 with the LiDAR component of the CAO (Carnegie Airborne Observatory, USA). The overall aim of the study was to analyze the capabilities and limitations of SAR data for woody cover mapping and the investigation of the potential synergistic use of LiDAR jointly with radar systems. Furthermore, the influence of seasonality for radar mapping of woody vegetation cover was investigated. The LiDAR-based woody cover was used for training and validation of the radar data.

The woody cover map based on the PALSAR L-band backscatter intensities (Fig. 16.27) was calculated using a Random Forest algorithm. The highest correlation to the reference data was obtained from the dry season satellite acquisitions (Fig. 16.25). The retrieved map was validated at a resolution of 50 m with $R^2 = 0.73$ and RMSE = 7.62 %. The results show promising sensitivity of L-band backscatter for mapping woody cover of savanna surfaces (compare Fig. 16.26).

16.4 Perspectives

Radar time series have led to innovative and unprecedented Earth observation products such as extended crop type mapping and above-ground forest growing stock (this Chapter), or – recently – global water bodies (Santoro and Wegmüller 2014) and the urban foot-print (Esch et al. 2013).

In the past, radar data were not available in the temporal or geometric resolution needed – or too expensive. Therefore, the knowledge created since the 1980s could not be transformed into operational routines – until now. With the new fleet of

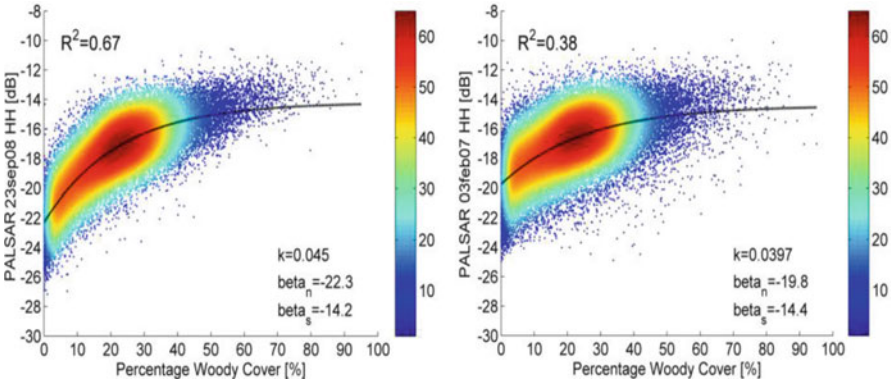

Fig. 16.25 Regression analysis between PALSAR L-band backscatter and airborne LiDAR-retrieved woody cover: .(*left*) winter dry season, (*right*) summer wet season (Urbazaev et al. 2013). Due to an increase of low vegetation and soil moisture during the wet season the backscatter intensity from low woody cover regions is increased and sensitivity to the woody components decreased. The dry season is therefore recommended for savanna woody cover mapping with L-band sensors

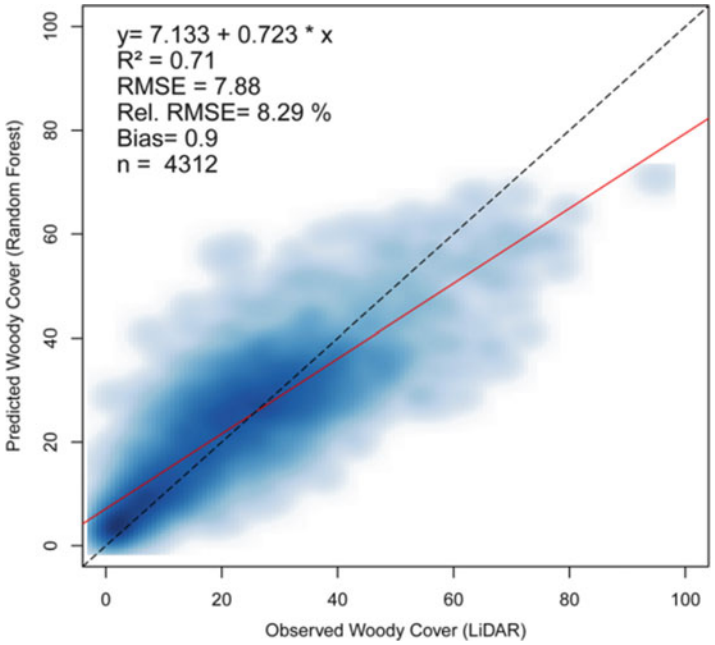

Fig. 16.26 PALSAR L-band predicted vs. airborne LiDAR-observed woody cover of undisturbed savanna vegetation in Kruger National Park, South Africa (Urbazaev et al. 2013). The red line indicates the regression line. The typical exponential behavior can be observed with a slight saturation effect above 60 % woody cover

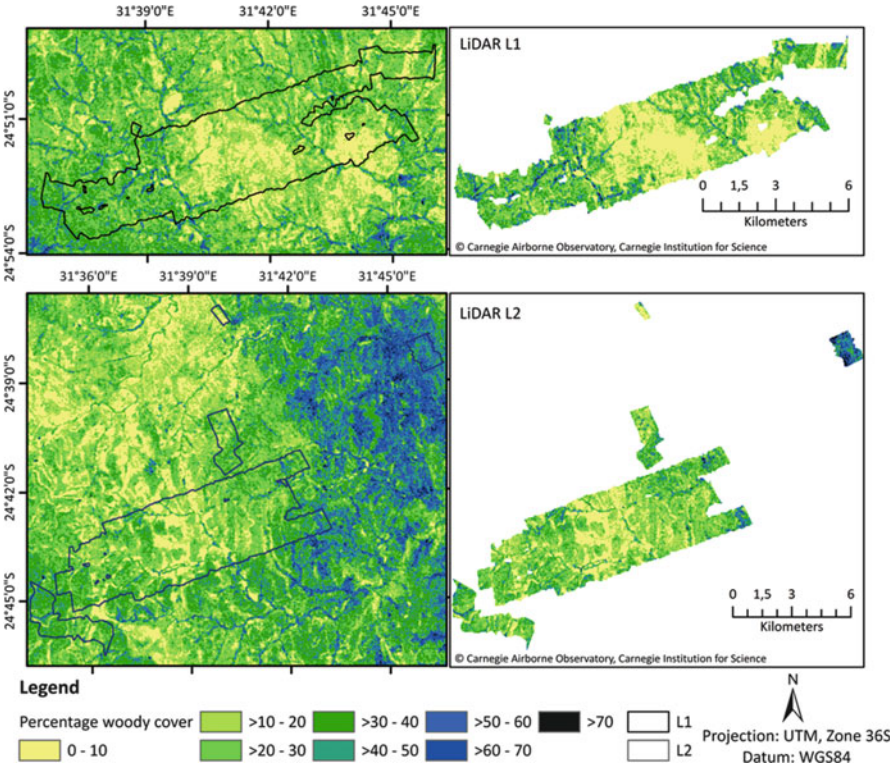

Fig. 16.27 Comparison between PALSAR-retrieved woody cover (*left*) and CAO LiDAR-based woody cover (*right*) for two sites in Kruger National Park, South Africa. Both spatial patterns are in very good agreement (Urbazaev et al. 2013)

active radar sensors being launched during this 2nd decade of the new millennium (ALOS-2 PALSAR, BIOMASS, COSMO-SkyMED Second Generation, RADARSAT Constellation, Sentinel-1a/-1b, TerraSAR Next Generation, and more planned), further very advanced analysis techniques such as differential and polarimetric SAR interferometry (DInSAR, PolInSAR), persistent scatterer interferometry (PSI) or radar tomography will become operational from space. Now, all advantages of microwave remote sensing such as independence from solar illumination, penetration capabilities through clouds and volumetric media, sensitivity to water content, capability to measure surface movements, etc. will lead to reliable Earth observation contributions. Such consistent observables are desperately needed for environmental models and model-data fusion methods to develop benchmarks (Thurner et al. 2013) or to constrain model calculations (Quegan et al. 2011) in an increasingly fast changing and complex world. Hence, the famous radar equation, which was mentioned in the introduction, will persist to be one of the most fundamental descriptions for Earth observation.

Acknowledgements The authors want to thank the funding agencies German Federal Minister of Education and Research (BMBF), Federal Ministry for Economic Affairs and Energy (BMWI), Alliance of Science Organisations in Germany (DFG), German Aerospace Centre (DLR), European Commission (EC), European Space Agency (ESA) and Japan Aerospace Exploration Agency's (JAXA) Kyoto & Carbon Initiative, who have facilitated through their support in funding and data supply our continuous progress in SAR applications for large-area land surface mapping.

References

Ackermann N (2015) Growing stock volume estimation in temperate forested areas using a fusion approach with SAR satellites imagery series: Springer theses XXV, 307 p 141, illus., 121 illus. in color. ISBN 978-3-319-13138-2

Ackermann N, Thiel C, Borgeaud M, Schmullius C (2010) Potential of fusion of SAR and Optical satellite imagery for biomass estimation in temperate forested areas. In: Proceedings of the ESA living planet symposium, 28 June–2 July 2010, Bergen, Norway. http://earth.eo.esa.int/workshops/livingplanetsymposium2010/sessions/CXNL_10a04_870140.htm. Accessed 30 Nov 2014

Askne J, Santoro M (2005) Multitemporal repeat pass SAR interferometry of boreal forests. IEEE Trans Geosci Remote Sens 43(6):1219–1228

Askne J, Dammert P, Ulander LMH, Smith G (1997) C-band repeat-pass interferometric SAR observations of forest. IEEE Trans Geosci Remote Sens 35:25–35

Attema EPW, Ulaby FT (1978) Vegetation modeled as a water cloud. Radio Sci 13(2):357–364

Balzter HC, Schmullius C (2001) Mapping Siberian forests. First boreal forest map of Siberia from spaceborne radar. GIM Int 15:40–43

Balzter HC, Talmon E, Wagner W, Gaveau D, Plummer S, Yu J, Quegan S, Davidson M, Le Toan T, Gluck M, Shvidenko A, Nilsson S, Tansey K, Luckmann A, Schmullius C (2002) Accuracy assessment of a large-scale forest cover map of Central Siberia from synthetic aperture radar. Can J Remote Sens 28(6):719–737

Cartus O, Eckardt R, Richter N (2008) GMES/Sentinel-1 analysis of multi-temporal land observation at C-band (AMOC ESTEC contract no. 21302/07/NL/CB). Final report, Department for Earth Observation, University Jena, Germany

Cartus O, Santoro M, Schmullius C, Li Z (2011) Large area forest stem volume mapping in the boreal zone using synergy of ERS-1/2 tandem coherence and MODIS vegetation continuous fields. Remote Sens Environ 115:931–943

Dobson MC, Ulaby FT, Le Toan T, Beaudoin A, Kasichke ES, Christensen N (1992) Dependence of radar backscatter on coniferous forest biomass. IEEE Trans Geosci Remote Sens 30:412–416

Eckardt R, Berger C, Thiel C, Schmullius C (2013) Removal of optically thick clouds from multi-spectral satellite images using multi-frequency SAR data. Remote Sens 5(6):2973–3006

Eriksson LEB, Santoro M, Wiesmann A, Schmullius C (2003) Multi-temporal JERS repeat-pass coherence for growing stock volume estimation of Siberian forest. IEEE Trans Geosci Remote Sens 41(7):1561–1570

Eriksson L, Askne J. Santoro M, Schmullius C, Wiesmann A (2005) Stem volume retrieval with spaceborne L-band repeat-pass coherence. Multi-temporal combination for boreal forest. In: Proceedings of IGARSS'05. Seoul, 25–29 July 2005, pp 3591–3594

Esch T, Marconcini M, Felbier A, Roth A, Heldens W, Huber M, Schwinger M, Taubenbock H, Muller A, Dech S (2013) Urban footprint processor—fully automated processing chain generating settlement masks from global data of the TanDEM-X mission. Geosci Remote Sens Lett 10(6):1617–1621

Hansen MC, DeFries RS, Townshend JRG, Carroll M, Dimiceli C, Sohlberg RA (2003) Global percent tree cover at a spatial resolution of 500 meters: first results of the MODIS vegetation continuous fields algorithm. Earth Interact 7(10):1–15

Henderson FM, Lewis AJ (1998) Principles and applications of imaging radar – manual of remote sensing, vol 2. Wiley, New York

Hüttich C, Stelmaszczuk-Górska MA, Eberle J, Kotzerke P, Schmullius C (2014a) Operational forest monitoring in Siberia using multi-source earth observation data. Sib J Forest Sci 5:38–53

Hüttich C, Korets M, Bartalev S, Zharko V, Schepaschenko D, Shvidenko A, Schmullius C (2014b) Exploiting growing stock volume maps for large scale forest resource assessment: cross-comparisons of ASAR- and PALSAR-based GSV estimates with forest inventory in central Siberia. Forests 5(7):1753–1776. doi:10.3390/f5071753

Leiterer R, Reiche J, Cartus O, Santoro M, Schmullius C, Li Z (2010): Multiscale Comparison of forest maps based on forest stem volume classification and existing land cover products. In: Proceedings of the 2010 dragon 2 symposium, 17–21 May 2010, Guilin, China

Luckmann A, Tansey K, Schmullius C (2004) The construction of ERS-tandem and JERS SAR image mosaics for large-scale mapping of boreal forest in Siberia. Int J Remote Sens 25:751–768

Quegan S, Yu JJ (2001) Recursive multi-channel filtering of SAR images. IEEE Trans Geosci Remote Sens 39(11):2373–2379

Quegan S, Le Toan T, Yu JJ, Ribbes F, Floury N (2000) Multitemporal ERS SAR analysis applied to forest monitoring. IEEE Trans Geosci Remote Sens 38(2):741–753

Quegan S, Beer C, Shvidenko A, McCallum I, Handoh I, Peylin P, Rödenbeck C, Lucht W, Nilsson S, Schmullius C (2011) Estimating the carbon balance of central Siberia using a landscape-ecosystem approach, atmospheric inversion and dynamic global vegetation models. Glob Chang Biol 17:351–365

Reiche J, Leiterer R, Cartus O, Santoro M, Schmullius C, Zengyuan L (2010) FOREST DRAGON 2: large-area forest stem volume mapping in China, using ERS-1/2 tandem coherence. In: Proceedings CD of ESA living planet symposium, 27 June–2 July 2010, Bergen, Norway

Riedel T, Thiel C, Schmullius C (2008) Fusion of multispectral optical and SAR images towards operational land cover mapping in Central Europe. In: Blaschke T, Lang S, Hay GJ (eds) Object-based image analysis – spatial concepts for knowledge-driven remote sensing applications. Springer, Berlin, pp 493–512

Rosenqvist A, Shimada M, Ito N, Watanbe M (2007) ALOS PALSAR: a pathfinder mission for global-scale monitoring of the environment. IEEE Trans Geosci Remote Sens 45 (11):3307–3316

Santoro M, Cartus O (2010) STSE-BIOMASAR: validating a novel biomass retrieval algorithm based on hyper-temporal wide-swath and global monitoring Envisat ASAR datasets. Final report, ESA ESRIN contract no. 21892/08/I-EC

Santoro M, Wegmüller U (2014) Multi-temporal synthetic aperture radar metrics applied to map open water bodies. J Select Top Appl Earth Obs Remote Sens 7(8):3225–3238. doi:10.1109/JSTARS.2013.2289301

Santoro M, Askne J, Smith G, Fransson JES (2002) Stem volume retrieval in boreal forests from ERS-1/2 interferometry. Remote Sens Environ 81:19–35

Santoro M, Beer C, Cartus O, Schmullius C, Shvidenko A, McCallum I, Wermüller U, Wiesmann A (2011) Retrieval of growing stock volume in boreal forest using hyper-temporal series of Envisat ASAR ScanSAR backscatter measurements. Remote Sens Environ 115(2):490–507

Santoro M, Cartus O, Fransson J, Shvidenko A, McCallum I, Hall R, Beaudoin A, Beer C, Schmullius C (2013a) Estimates of forest growing stock volume for Sweden, Central Siberia, and Québec using Envisat advanced synthetic aperture radar backscatter data. Remote Sens 5:4503–4532

Santoro M, Schmullius C, Pathe C Schwilk J, Beer C, Thurner M, Fransson JES, Shvidenko A, Schepaschenko D, McCallum I, Beaudoin A, Hall R (2013b) Estimates of forest growing stock volume of the Northern Hemisphere from Envisat ASAR. In: Proceedings of the living planet

symposium 1. http://biomasar.org/fileadmin/biomasar/papers/2849916santoro.pdf. Accessed 30 Nov 2014

Santoro M, Beaudoin A, Beer C, Cartus O, Fransson J, Hall R, Pathe C, Schmullius C, Shvidenko A, Thurner M, Wegmuller U (2015) Forest growing stock volume of the northern hemisphere: spatially explicit estimates for 2010 derived from Envisat ASAR data. Remote Sens Environ (in review)

Schmullius C (1997) Monitoring Siberian forests and agriculture with the ERS-1 Windscatterometer. IEEE Trans Geosci Remote Sens 35(5):1363–1366

Schmullius C, Rosenqvist A (1997) Closing the gap – a Siberian boreal forest map with ERS-1/2 and JERS-1. 3rd ERS symposium on space at the service of the environment, Florence, 17–21 March, 1997. http://earth.esa.int/workshops/ers97/papers/schmullius/. Accessed 30 Nov 2014

Schmullius C, Baker JS, Balzter H, Davidson M, Eriksson L, Gaveau D, Gluck M, Holz A, Luckman A, Marschalk U, McCallum I, Nilsson S, Oeskog A, Quegan S, Rauste Y, Roth A, Shvidenko A, Skuding V, Strozzi T, Tansey K, Vietmeier J, Voloshuk L, Wagner W, Wegmüller U, Wiesmann A (2001) SIBERIA – SAR imaging for boreal ecology and radar interferometry applications. Final report. EC Center for Earth Observation, project reports, contract no. ENV4-CT97-0743-SIBERIA. http://www.siberia1.uni-jena.de. Accessed 30 Nov 2014

Schmullius C, Leiterer R, Burjack I, Traut K, Santoro M, Li ZY, Ling FL (2012) FOREST DRAGON-2 – final results of the european partners. In: Dragon-2 final results & dragon 3 Kick-off symposium, Beijing, China. http://www.zora.uzh.ch/77312/. Accessed 30 Nov 2014

Thiel C (2010) GMES/Sentinel-1: software and prototyping of level 2 products for land-use-mapping analysis of multi-temporal land observation at C-band (AMOC II – ESA CONTRACT C21302/07/NL/CB). Final report, Department for Earth Observation, University Jena, Germany

Thiel C, Schmullius C (2013a) Investigating the impact of freezing on the ALOS PALSAR InSAR phase over Siberian forests. Remote Sens Lett 4(9):900–909

Thiel C, Schmullius C (2013b) Investigating ALOS PALSAR interferometric coherence in central Siberia at unfrozen and frozen conditions. Can J Remote Sens 39(3):232–250

Thiel C, Schmullius C (2014) Impact of tree species on magnitude of PALSAR interferometric coherence over Siberian forest at frozen and unfrozen conditions. Remote Sens 6:1124–1136. doi:10.3390/rs6021124

Thiel C, Thiel C, Riedel T, Schmullius C (2007) Analysis of ASAR APP time series over Siberia for optimising forest cover mapping – a GSE forest monitoring study. In: Proceedings CD of 6th ESA Envisat symposium, 23–27 April 2007, Montreux, Switzerland. https://earth.esa.int/workshops/envisatsymposium/proceedings/sessions/3D4/451296th.pdf. Accessed 30 Nov 2014

Thiel C, Thiel C, Riedel T, Schmullius C (2008) Object based classification of SAR data for the delineation of forest cover maps and the detection of deforestation – a viable procedure and its application in GSE forest monitoring. In: Blaschke T, Lang S, Hay GJ (eds) Object-based image analysis – spatial concepts for knowledge-driven remote sensing applications. Springer, Berlin, pp 327–344

Thiel C, Santoro M, Cartus O, Thiel C, Riedel T, Schmullius C (2009a) Perspectives of SAR based forest cover, forest cover change and biomass mapping. In: Vasse CP (ed) The Kyoto protocol: economic assessments, implementation mechanisms, and policy implications. Nova Science Publishers, New York, pp 13–56

Thiel C, Thiel C, Schmullius C (2009b) Operational large area forest monitoring in Siberia using ALOS PALSAR summer intensities and winter coherence. IEEE Trans Geosci Remote Sens 47 (12):3993–4000

Thiel Ca, Cartus O, Eckardt R, Richter N, Thiel Ch, Schmullius C (2009c) Analysis of multi-temporal land observation at C-band. IEEE geoscience and remote sensing symposium (IGARSS) III, pp 318–321. http://dx.doi.org/10.1109/IGARSS.2009.5417764

Thurner M, Beer C, Santoro M, Carvalhais N, Wutzler T, Schepaschenko D, Shvidenko A, Kompter E, Ahrens B, Levick S, Schmullius C (2013) Carbon stock and density of northern boreal and temperate forests. Glob Ecol Biogeogr 23(3):297–310

Ulaby FT, Moore RK, Fung AK (1986) Microwave remote sensing: active and passive, vol. III – volume scattering and emission theory, advanced systems and applications. Artech House, Inc., Dedham

Urbazaev M, Schmullius C, Thiel C, Renaud M, Naidoo L, Levick S, Smit I, Asner G, Leblon B (2013) Delineation of woody cover by using full and dual polarimetric L- and C-band datasets in the Kruger National Park, SA. In: ESA living planet symposium, Edinburgh, 9–-13 September 2013. http://seom.esa.int/LPS13/5867d0b0/LP_2013_Urbazaev.pdf. Accessed 30 Nov 2014

Wagner W, Luckman A, Vietmeier J, Tansey K, Baltzer H, Schmullius C, Davidson M, Gaveau D, Gluck M, Letoan T, Quegan S, Shvidenko A, Wiesman A, Yu JJ (2003) Large-scale mapping of boreal forest in SIBERIA using ERS tandem coherence and JERS backscatter data. Remote Sens Environ 85:125–144

Wooding M, Attema E, Aschbacher J, Borgeaud M, Cordey RA, De Groot H, Harms J, Lichtenegger J, Nieuwenhuis G, Schmullius C, Zmuda A (1995) Satellite radar in agriculture. Experience with ERS-1. ESA Scientific Publications, Noordwijk